Single-Channel Stereoscopic Imaging System Using Rotating Deflector

Won Hyuk Jang

The Graduate School

Yonsei University

Department of Biomedical Engineering

Single-channel Stereoscopic Imaging System Using Rotating Deflector

A Master's Thesis

Submitted to the Department of Biomedical Engineering

and the Graduate School of Yonsei University

in partial fulfillment of the

requirements for the degree of

Master of Biomedical Engineering

Won Hyuk Jang

January 2014

This certifies that the master's thesis of
Won Hyuk Jang is approved.

_____

Thesis Supervisor: [Byungjo Jung]

_____

[Dong Youn Kim]

_____

[Kyung Hwan Kim]

The Graduate School
Yonsei University
January 2014

Acknowledgments

This thesis marks the end of my journey with the completion of my M.S. I have not traveled in a vacuum on this journey. The work presented in this thesis would not have been possible without my close association with many people who were always there when I needed them the most. I take this opportunity to acknowledge them and extend my sincere gratitude for helping me. I take this moment to thank the people around me.

Foremost, I would like to express my sincere gratitude to my advisor, Prof. Byungjo Jung, for his excellent guidance, patience, and motivation. He has been there for the last two years, motivating and inspiring me toward new possibilities in life. I will never find words to say what I owe to him, and if I started doing it, I would not know where to stop.

I would like to acknowledge my BOL colleagues: Heesung Kang, Taeyoon Son, Edalat Radfar, Jihoon Park, and Eunkwon Jun. They have taught me the lab culture and shown me by example how to understand the hard facts of life. They have influenced me not only in academic life but also in my social life. I will never forget what I have learned through them.

I extend my thanks to both my junior and senior friends from Yonsei University and Yonsei University Graduate School. Special thanks to Kwangsu Cha and Bora Jeong for always being good friends. Compared with many friends, I have taken a slightly different path, allowing me to earn my B.S. and M.S. earlier. Because of my early graduation, I have sometimes been a mentor to friends who needed me. It was a chance to look back into my life. I hope my advice was helpful.

Among many friends from Seohyun High School, I would especially like to thank “Panic Blu” for being there during my ups and downs. After six years of unchanging friendship, I expect it to last.

Last but not least, I would like to thank my family, who provided a carefree environment for me and who encouraged and helped me at every stage of my academic life. Although they may not understand the research I performed, they have always supported my decision.

Won Hyuk Jang

Table of Contents

List of Figures

List of Tables

List of Equation

Abstract

In a conventional dual-channel stereoscopic imaging system (SIS), two cameras are often used to take images at different visual orientations, creating a three-dimensional (3D) image. Because two cameras are used, visual fatigue may be caused by differences between the cameras involving temporal synchronization, geometrical calibration, and color balance. Furthermore, owing to its mechanical composition, the imaging system is generally bulky.

To eliminate the possible limitations of current conventional dual-camera SISs, research was conducted to develop a 3D SIS using a single camera. Its purpose is to create image disparity (ID), a key factor in producing stereoscopic images. Using a transparent rotating deflector (TRD), ID was mimicked assuming that light refraction through the TRD would create the necessary ID.

First, the system's efficacy was tested using a thorough simulation and experiment based on Snell's law. Light propagation through the TRD was modeled using ZEMAX. The ID was calculated for various TRD refractive indices and thicknesses. On the basis of the simulation and calculation, a TRD-based SIS (TRD-SIS) was developed using manual rotation of the TRD. Second, a real-time TRD-SIS was set up to allow real-time stereoscopic imaging and display. A complementary metal–oxide–semiconductor (CMOS) camera was used along with a stepping motor controlled by a microcontroller unit. The acquired images were visualized in 3D using an active 3D method. Finally, the system was evaluated in terms of two factors: (1) temperature generation and (2) the image characteristics. The temperature changes in the optical components were measured at the motor surface and motor driver. The image characteristics were evaluated by calculating

the coefficient of variation of acquired images of a white reflectance target. In addition, a method of controlling heat generation using a heat sink and motor fan was devised.

Keywords: 3D image, stereoscopic image, single-channel, transparent rotating deflector

1. Introduction

Stereoscopy (also called stereoscopic imaging) is a technique for creating depth information or the illusion of depth in two-dimensional (2D) images by using stereopsis originating in light patterns, relative sizes, overlapping, shade, color, and movement analysis. In the human eye and in optical systems, 2D images are created at the left and right eye and then processed in the brain to yield depth information.

The first concept for a stereoscopic method was introduced in 1838 by *Sir Charles Wheatstone*.(Welling 1978) Scientific and technological development of three-dimensional (3D) stereoscopic imaging techniques have widened its application in a variety of fields, including medicine, laparoscopy, endoscopy, and even cinema.(Cuschieri 1991, 404-407, Welling 1978)

The optical setups of a 3D imaging system are organized using either dual or single channels. A dual-channel system generally uses two different cameras for stereoscopic imaging, whereas a single-channel system is designed with a single camera. Both optical setups have advantages and disadvantages and can be used for different purposes.(van Bergen, Kunert, and Buess 1999, 732-737) Most conventional 3D stereoscopic imaging system (SIS) have been based on dual-channel video technology (Szold 2005, 730-733), which consists of two cameras. Although significant benefits of the technology have been demonstrated (Chan et al. 1997, 438-440, Hofmeister et al. 2001, 12-24, Taffinder et al. 1999, 1087-1092, van Bergen, Kunert, and Buess 1999, 732-737), severe limitations still exist because of its optical system design. Owing to these limitations, viewers of dual-channel stereoscopic systems are continuously exposed to the clinical side effects of headaches, nausea, ocular fatigue, and dizziness.(Chan et al. 1997, 438-440, McDougall

et al. 1996, 371-374, Mitsuhashi 1996, 1344-1356, van Bergen, Kunert, and Buess 1999, 732-737) Such clinical side-effects may be caused by 1) image mismatch due to optical axis mismatch between the two separate cameras; 2) mismatch in image characteristics such as exposure, color, and brightness; and 3) geometrical mismatch of the detectors, such as rotational errors, size differences, and vertical and horizontal shift.

To overcome these limitations, a planar catadioptric stereo system was realized using a single camera.(Wu 2007, 686-698) Single-channel stereoscopic imaging technologies such as a shutter mechanism and insect eye technology were developed by *Storz* (KARL STORZ 3D System, STORZ) and *Visionsense* (VSII, Visionsense).(Szold 2005, 730-733) However, these technologies also have limitations, as follows: 1) the shutter mechanism produces weak 3D perception because of small unpredictable image changes generated by a single optical detector; and 2) the insect eye technology has been limited by its low image intensity, which originates from its microlens array.

Another method of image disparity (ID) generation was studied by various research groups.(Chunyu, and Ahuja 2004, 108-111 Vol.4, 2006, 2316-2323, DooHyun, and Inso 2000, 528-541, Teoh, and Zhang 1984, 186-189) *Lee* et al. created ID within a single camera by placing a bi-prism in front of the camera. By using refraction caused by the prism, the ID is detected in the single camera. However, owing to the use of the bi-prism, the resolution of the detected object seems to be halved.(DooHyun, and Inso 2000, 528-541)

Research using a parallel planar plate, or transparent plate, which has equivalent optical characteristics to the proposed transparent rotating deflector (TRD), was presented by different workgroups.(Choi, Rubtsov, and Kim 2012, 926-933, Chunyu, and Ahuja 2004, 108-111 Vol.4, 2006, 2316-2323) Research led by *Chunya* et al. focused on the

reconstruction of depth information using the detected image, whereas in the work of *Choi* et al., it was used to measure the size of an object.

The present study aimed to develop an imaging system allowing real-time visualization of 3D images using a single camera. First, the feasibility of inducing ID was confirmed by a simulation and experimental analysis using the optical setup of the TRD stereoscopic imaging system (SIS). Second, a real-time TRD-SIS using a stepping motor and an active 3D method was devised.

2. Background Theory

2.1 The Law of Refraction

Snell's law (figure 1) is used to describe the relationship between incident and refracted light. It describes light passing through a boundary between two different media. Snell's law states that the ratio of the sines of the angles of incident and refracted light is equivalent to the ratio of the phase velocities in two media or to the reciprocal of the ratio of the indices of refraction. (Hecht 2002)

$$n_1 sin\theta_1 = n_2 sin\theta_2 \quad (1)$$

Snell's law is used to determine the direction of light rays through refractive media with varying indices of refraction. The indices of refraction of the media are used to represent the factor by which a light ray's speed decreases when traveling through a refractive medium, such as glass or water, compared to its velocity in a vacuum.

As light passes the border between media, depending upon the relative refractive indices of the two media, the light will be refracted to either a lesser angle or a greater one. These angles are measured with respect to the normal line perpendicular to the boundary. Light traveling from air into water is refracted toward the normal line because light is slowed down in water; light traveling from water to air would refract away from the normal line.

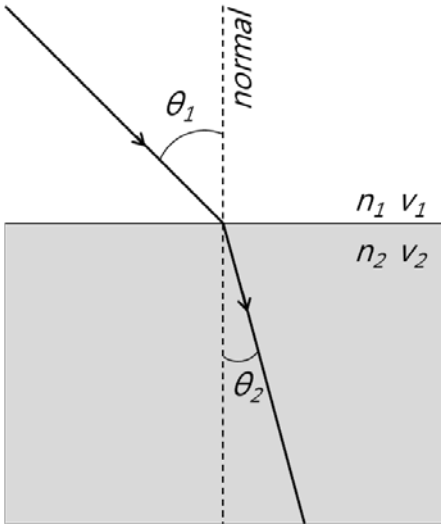

Figure 1. Snell's law of refraction

Refraction between two surfaces is also referred to as reversible because if all the conditions were identical, the angles would be the same for light propagation in the opposite direction.

2.2 Depth Cues

The key factors of visual perception of depth are called depth cues and are critical factors allowing the recognition of 3D images. Depth cues do not act individually but in relation to each other with continuous augmentation by human sensation. Various depth cues arise from the nature of object detection. In addition to the depth cues derived from image detection, some depth cues arise internally. Internal depth cues are based on signals from the brain due to past experience, association, or expectation. Depth cues can be subcategorized in several ways: monocular and binocular cues(Goldstein 1999), as shown in table 1, and egocentric and relative cues(Wade, and Swanston 2013). Some people,

who cannot process and perceive depth cues, lack the ability to recognize 3D images.(Blundell, and Schwarz 2000)

Monocular Cues	Occlusion
	Linear Perspective
	Aerial Perspective
	Lighting and Shading
	Height in the Visual Field (Elevation)
	Binocular Parallax
	Motion Parallax
	Relative/Familiar Size
	Accommodation
	Kinetic Depth Effect
Binocular Cues	Stereopsis
	Convergence
	Shadow Stereopsis

Table 1. Classification of Depth Cues

- Binocular Parallax: Owing to the slightly different locations of the eyes, which are approximately 60–65 mm apart, each eye has a slightly different perspective on an object. Within the brain, the disparity between the two different images is processed and fused to generate relative depth information. Depending on the distance to the object, the binocular disparity may not provide sufficient information.
- Motion Parallax: The relative motion between two objects differs depending on the distance to the objects. During constant movement of the viewer, an object closer to the viewer may appear to move farther across the visual field than an object located farther in the distance.
- Linear Perspective: Objects at a distance from the viewer seem to converge, allowing us to reconstruct their relative distances.

- Occlusion: The placement of opaque objects may cause overlapping of the placed objects. Specifically, the first object may overlap the second object, making the latter invisible to the viewer. On the basis of the overlap, the brain assumes that the invisible object lies behind the first object.
- Lighting and Shading: The shadows and shading of an object provide information about its form, surface structure, surface texture, and position relative to the environment.
- Aerial Perspective: Light scattering and absorption caused by particles in the air cause an object to look blurry and dull in proportion to its distance. Owing to the properties of light scattering, the overall image tends to look bluer than the original image.
- Height in Visual Field: The vertical positioning of objects, usually above horizon, is interpreted to be further away. Objects at a higher scene are as being farther away.
- Accommodation: The relaxation and tensing of the ciliary muscle contributes to physiological depth cues. The focus of the eye is adjusted depending on the distance to the object, changing the shape of the lens. The brain processes the magnitude of the tension applied to the eye, generating depth information. However, the shape of the lens is nearly constant for objects more than 10 m away, so this depth cue is limited.
- Convergence: The two eyes are controlled by the brain, which adjusts the muscular force exerted on the eyes. The eyes are swiveled inward to focus on the center of the object of interest.

- Relative/Familiar Size: On the basis of previous experience, the relative size of the object of interest can be predicted.

2.3 Stereoscopy

Stereoscopy is the generation of 3D image from 2D images. It is known as the enhancement of depth perception in the detected image. In most cases, the two detected images have a slight offset, known as image disparity (ID). In humans, the two eyes allow the detection of two different images (figure 2). In most cases the inter-ocular distance, or the distance between two human eyes, ranges between 6065 mm.(Durrani, and Preminger 1995, 237-247) When the eyes focus on an object, an angle of convergence (α) is formed, and the object is detected at two different visual orientations. Depending on the distance to the object, the angle of convergence changes through accommodation and changes the optical power of the eye.(Hofmeister et al. 2001, 12-24)

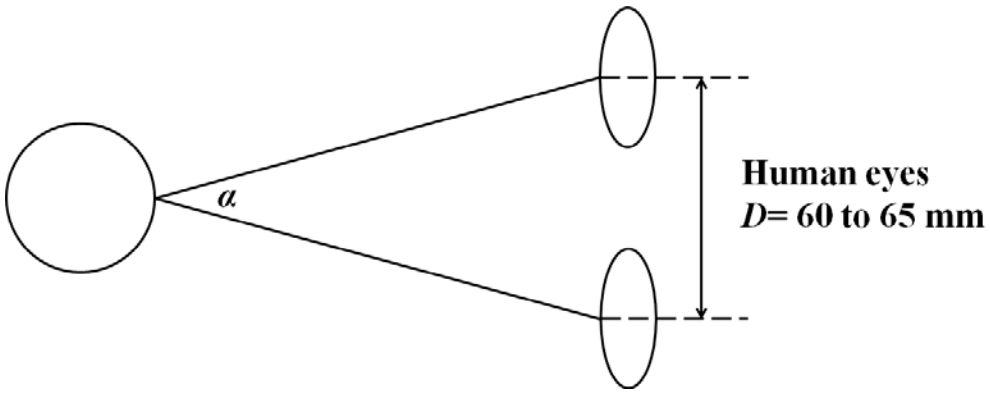

Figure 2. Human stereoscopic viewing conditions

2.4 3D Display

3D stereoscopic images can be visualized using several methods: passive 3D, active 3D, head-mounted displays (HMDs), autostereoscopic displays, and immaterial displays.(Hong et al. 2011, H87-H115) Passive 3D, active 3D, and HMDs require an additional visual aid to project left and right images to the left and right eyes, respectively; however, autostereoscopic and immaterial displays require no visual aid.

Passive 3D uses polarized film to control the images shown to the eye. Such a system consists of passive shutter glasses (polarized glasses, figure 3) paired with a display screen.(Sexton, and Surman 1999, 85-99) Both the left and right images are displayed simultaneously; through polarization, the left and right images are selectively detected in each eye. The glass lenses are polarized perpendicular to each other to allow the detection of specific images without other images overlapping. Passive shutter glasses are relatively inexpensive to manufacture, and multiple people can view 3D image simultaneously. However, because of its fixed polarization characteristics, the visualized 3D image's intensity and resolution are reduced.

Figure 3. Passive 3D glasses (LK3D9117C1, Ray-Ban)

Active 3D uses a liquid crystal to control the image shown to the eye. An active 3D system, similar to a passive 3D system, consists of active shutter glasses (figure 4) and a paired display screen. The active shutter glasses consist of a polarized film and a liquid crystal, the polarization of which is changed according to the input voltage. The glass is perpendicularly polarized by applying a voltage to the active shutter glasses, making the glass opaque.(Srivastava, de Bougrenet de la Tocnaye, and Dupont 2010, 522-530) By controlling the opacity of the glass, the detected image is mechanically controlled, allowing the visualization of 3D images. In wireless active 3D, the active shutter glasses and display screen are paired using infrared signals. The display screen is absolutely synchronized with the active shutter glasses. Compared to the passive 3D system, the optical glasses are more costly to manufacture.

Figure 4. Active 3D (3D Vision, NVIDIA)

An HMD (figure 5) consist of a pair of liquid crystal displays or cathode ray tubes that are mounted on the head to show 3D images to the observer.(Shibata 2002, 57-64) Despite the disadvantages of wearing the display, in some cases it is a commonly selected method of 3D image display. HMDs have several characteristics: (1) large images can be

used, (2) the overall system size can be reduced, and (3) when a transparent HMD is used, a superimposed image can be observed.

Figure 5. Head-mounted display (HMZT1, Sony)

Unlike passive 3D and active 3D, the autostereoscopic method does not require an additional visual aid device.(Dodgson 2005, 31-36) Without using any visual aid, the 3D display shows a different image to each eye. Because no additional visual aid is needed, 3D images can be comfortably visualized; however, in some cases the 3D image is visualized only at fixed points.(Ezra et al. 1995, 31-40) The autostereoscopic method can be realized using a number of technologies: the parallax barrier, lenticular lens, and integral imaging.(Hong et al. 2011, H87-H115) In addition, the detected 3D images are known to lack resolution, color reproduction, and surface reproduction.(Hutarew, Moser, and Dietze 2004, 206-213)

An immaterial display is another option for displaying 3D images; however, it does not use an electronic display screen but displays 3D images immaterially.(Hong et al. 2011, H87-H115, Palovuori, and Rakkolainen 2012, 175-177) It is most frequently used in entertainment, and water and smoke are the most widely selected methods of displaying a 3D image.(DiVerdi et al. 2006, 605519-605519-10) As stated in research by *Rakkolaine*,

the turbulent flow in the medium plays a critical role in the resolution of the detected image; thus, this type of display represents a very difficult fluid mechanics task.(Rakkolainen, and Lugmayr 2007, 95-98)

2.5 Coefficient of Variation

In many studies, the coefficient of variation (CV) is a statistical measurement that is widely used to compare the variations between work groups. In science, the CV is applied in various fields, including mechanical design, signal processing, taxonomy, cultural science, and biology. (Bendel et al. 1989, 394-400, Cope, and Lacy 1995, 549-576, He, and Oyadiji 2001, 374-378, Toichi et al. 1997, 79-84, Wang, Goodpaster, and Kennedy 2013, 9-16) Furthermore, the CV is used to analyze the properties of light illumination in the optical system.(Qin et al. 2010, 17460-17476)

The CV is generally calculated as

$$\mathrm{CV} = \frac{S}{\overline{M}} \tag{2}$$

where *S* and *M* represent the standard deviation and mean, respectively.(Abdi 2010, 169-171) The CV is sometimes represented as a percentage:

$$\mathrm{CV} = \frac{S}{\overline{M}} \times 100 \tag{3}$$

3. Materials and Method

3.1 System Simulation

To validate the possibility of using a transparent rotating deflector (TRD) to create an image disparity (ID), a simulation was performed. The ID is defined as the lateral displacement between a reference point (initial optical axes) and refracted light. The ID caused by light refraction can be calculated using Snell's law (the law of refraction):

$$d = t \sin I \left[1 - \sqrt{\frac{1 - (\sin I)^2}{n^2 - (\sin I)^2}} \right] \tag{4}$$

where *d* represents the ID due to the TRD, *t* is the thickness of the TRD, *I* represents the incident angle of light at the surface of the TRD, and *n* is the refractive index of the TRD.(Chunyu, and Ahuja 2004, 108-111 Vol.4, Smith 2000) As shown in figure 6, the optical axis is labeled $\overline{AD}$; an actual light ray is represented by $\overline{AOCE}$, and $\overline{BC}$ represents the ID. At a fixed thickness (*t*), the ID ($\overline{BC}$) depends on the angle ∠FOC. When a material with a high refractive index (*n*) is used, the angle ∠FOC is small because of refraction. The refracted light $\overline{CE}$ is parallel to the incident light.

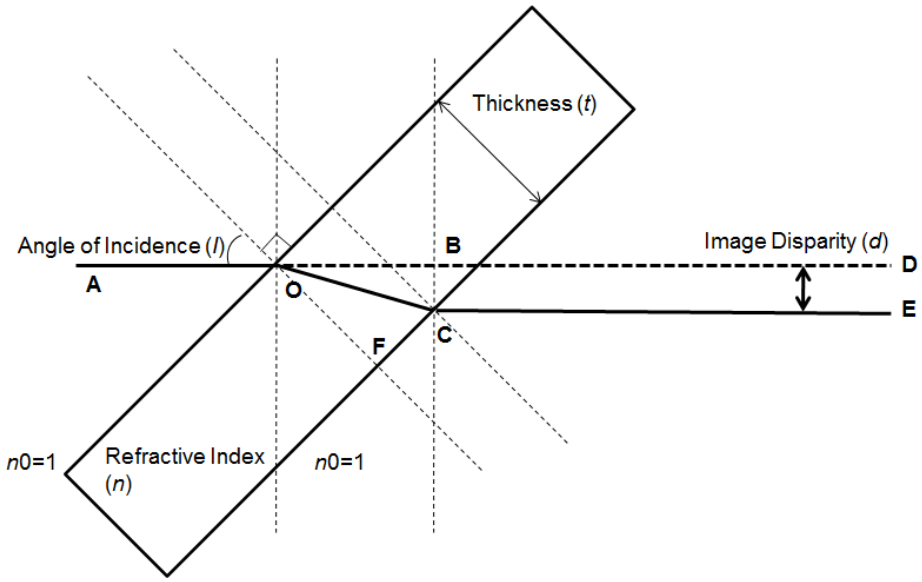

Figure 6. Image disparity based on Snell's law

A simulation was performed to verify the relation between the rotation angle and thickness of the TRD. Three different materials (acrylic plate, BK7, and diamond) were simulated at different TRD thicknesses (10 mm, 30 mm, 50 mm) at rotation angles of 0° to 80°. To visually verify the generation of ID, ZEMAX (ZEMAX-EE, ZEMAX) was used to simulate image propagation under constant conditions.

3.2 Image Disparity Experiment

A previously developed imaging system was adopted for experimental analysis of the ID.(Younwoo 2011, 138) The validity of 3D imaging using an optical window was analyzed using manual rotation of the optical window. The optical window was made of transparent acryl (n = 1.49) and was designed to be large enough to cover marginal rays. A Canon digital single-lens reflex (DSLR) camera (Canon EOS 350D, Canon Inc., Tokyo, Japan) with a Tamron zoom lens (AF28-300 mm, F/3.5–6.3, Tamron, Japan) was used as

the imaging device. Images were taken at two different visual orientations at equal rotation angles in different directions.

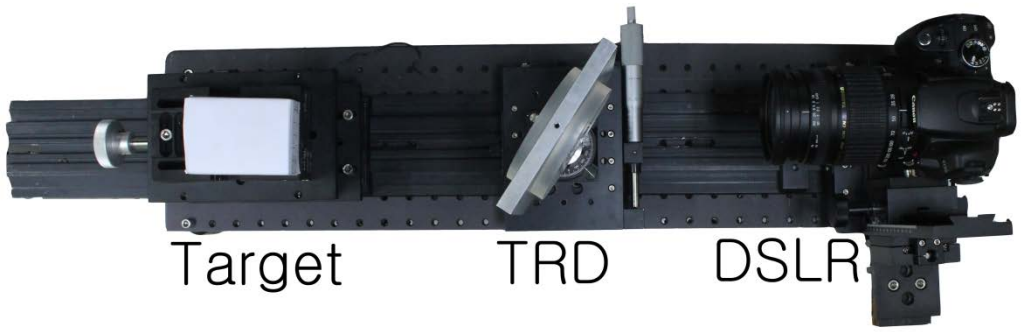

Figure 7. TRD-based stereoscopic imaging system (TRD-SIS)

Figure 7 shows the optical setup of the optical-window-based 3D stereoscopic imaging system (SIS), which consists of an object, an optical window, and a DSLR with a zoom lens. An optical window 30 mm in thickness was fabricated using acrylic glass. The ID was created by rotating the optical window when images were taken at two different visual orientations.

The left and right images were captured in three different ways depending on the direction of rotation: 1) half of the total angle equally rotated both clockwise and counterclockwise (denoted by H), 2) total angle rotated counterclockwise (denoted by R), 3) total angle rotated clockwise (denoted by L).

To analyze the 3D SIS, the rotation angle of the optical window was adjusted from 10° to 80° in 10° intervals, and 3D stereoscopic images were taken. Images were taken at the rotation directions of L, R, and H for each rotation angle. For precise analysis, the

experiment was performed at two different working distances (WD), 153 mm and 250 mm.

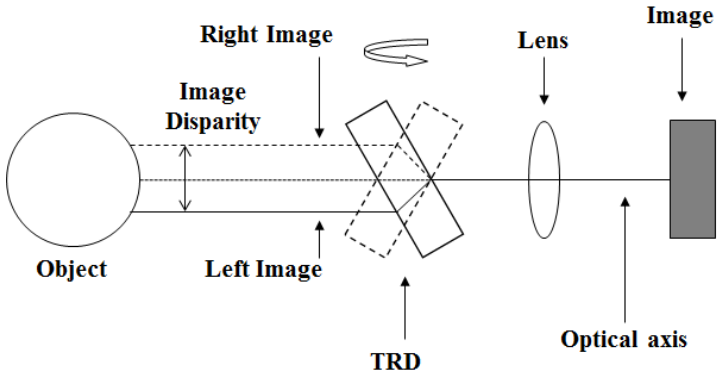

Figure 8. Expected image ray propagation. Images of the object are acquired at two different visual points.

A target object with ruler markings was used to acquire images at different rotation angles, which were used to define the ID. Anaglyphs, an encoding method of each eye's using opposite chromatic color filter, as shown in figure 8.

3.3 Real-time 3D Imaging System

On the basis of ID verification, a system was devised to achieve real-time 3D image visualization. In the design of the 3D imaging system, several components were chosen: a complementary metal–oxide–semiconductor (CMOS) camera sensor, stepping motor, and active shutter glasses. In addition, the camera hardware triggering function of the CMOS camera was used to acquire the image at a given time. The listed components were synchronized for exact and precise control using a centralized control system.

3.3.1 Microcontroller unit (MCU)

To perceive an adequate 3D image, all of the system components should be synchronized. A convenient method of synchronization is the use of a central control system, which can easily control the entire system. For this application, a microcontroller unit (MCU, figure 9, Atmel® AVR®) was chosen as the central control unit. To control the system components, general-purpose input/output was connected to the devices. Several optical system components were controlled: the camera, stepping motor driver, stepping motor, and 3D active shutter glasses. The embedded software was written in C.

Figure 9. Microcontroller unit (MCU, AtMega128, Atmel® AVR®)

3.3.2 Rotation methods

To allow real-time imaging with the proposed system, a method of continuous rotation had to be implemented. Owing to the optical design of the 3D stereoscopic system, a single-axis rotation had to be considered and validated. Among various possibilities for single-axis rotation, a galvanometer and stepping motor were chosen.

3.3.2.1 Galvanometer

A galvanometer is a sensitive ammeter that detects electrical current. It produces a rotary deflection caused by an analog electromechanical actuator in relation to the electrical current running through the coil. The deflection is proportional to the input signal. The structure of a galvanometer consists of an optical mirror mounted on the rotation axis.

The operation of the galvanometer differs greatly depending on the electrical signal input to it. To control the electrical signal input to the galvanometer, a specially tuned driver for a specific galvanometer has to be used. The input current is altered using this galvanometer driver, allowing various rotations of the optical mirror.

The galvanometer (6260H, Cambridge Technology) was controlled using a conventional function generator (DS340, Stanford Research Systems) and an analog servo driver (671 Servo Driver, Cambridge Technology), as shown in figure 10.

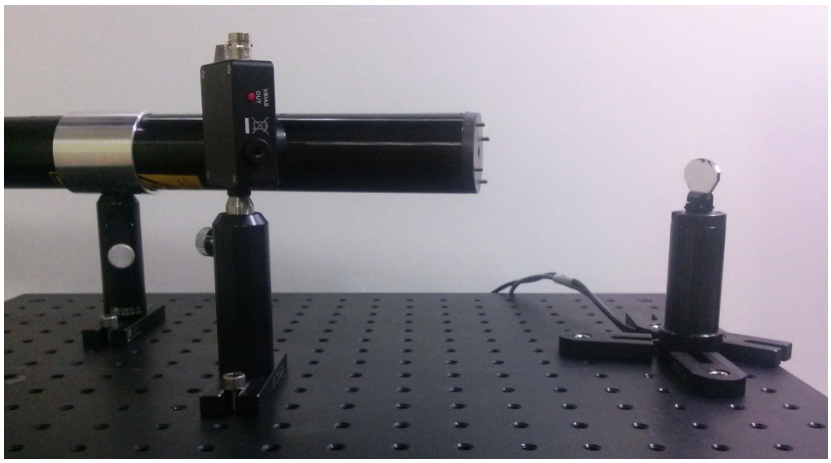

Figure 10. Test of galvanometer characteristics using laser source, galvanometer, and photodetector

The repeatability of the galvanometer under different control signals was tested. Using a laser source (10 mW, 633 nm, 1126P, JDS Uniphase) and a photodetector (DET 36A/M, Thorlab), the repeatability of the galvanometer was examined. The laser was guided to the rotating mirror on the galvanometer, and the reflected light was detected at two different spots, the center and the edge. Three different input frequencies were set as the input signal: 30 Hz, 60 Hz, and 120 Hz. Regardless of the input control signal, the rotation of the galvanometer was consistent.

3.3.2.2 Stepping motor and motor driver

Among the possible methods, a stepping motor (figure 11, A4K-M245, Autonics) and a controlling driver (MAI-2MT-ST V2.1, M.A.I.) were also selected. The rotation speed and direction of the stepping motor depend on the driver used and its input signal to the driver. The step angle in many cases is fixed as specified in the motor specification. The motor used here has a step angle of 1.8°, which as a result requires 11 input clocks to rotate 19.8°. Because the step angle is fixed at 1.8°, the total rotation angle is a constant multiple of the step angle.

To create continuous 3D images, 2D images of an object should be continuously acquired at two different visual orientations. Because two images of an object (left and right images) create one 3D image, pairs of left and right images were considered. In a single rotation cycle of the stepping motor, two images were taken. As a result, the motor rotation cycle per second has a critical impact on the frame rate of the final 3D image.

Figure 11. Stepping motor (A4K-M245, Autonics)

3.3.3 Transparent rotating deflector (TRD) and TRD mount

On the basis of the results of the ID experiment, a TRD was created using BK7. To accurately mount the TRD on the axis of the motor, a TRD mount was designed. The estimated specifications of the TRD mount required that it be as light as possible and remain on the motor axis even during rapid rotation.

3.3.4 Camera

To create a real-time continuous 3D image, the specified ideal 3D image display frequency has to be satisfied. Specifically, in normal humans, images of less than 24 fps are mostly recognized as discontinuous, but images of 24 fps or higher are considered to be continuous. To achieve a continuous real-time 3D image, a camera with a sufficient frame rate is required. In this research, a CMOS camera (acA2000-50gm NIR, Basler) was used to capture the images. The camera and its sensor sensitivity are shown in figures 12 and 13, respectively, and its specifications are listed in table 2.

Specifications	
Image Type	Mono
Model	acA2000-50gm NIR
Sensor Type	CMOS
Sensor Size	2/3 in.

Resolution	2048 * 1088
Pixel Size	5.5 µm * 5.5 µm
Frame Rate	50 fps
Interface	GigE

Table 2. Specifications of acA2000 50gm-NIR

Figure 12. acA2000 50gm-NIR, Basler

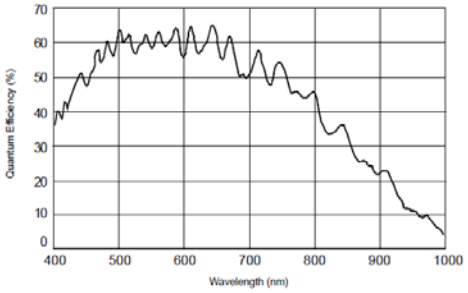

Figure 13. Camera sensor sensitivity

3.3.4.1 Camera trigger

To acquire a focused image between the rotation intervals of the stepping motor, a trigger that forces acquisition by the camera is required. Software and hardware triggers are most commonly used. A software trigger uses internal software or camera control software to specify the moment of image acquisition, whereas a hardware trigger uses an external signal to control image acquisition. Because a centralized control system was used, the hardware trigger function of the camera seemed to be suitable. For the camera used here, the suggested input voltage range is defined as 2.2–30 V. Signals outside the suggested range could cause the camera to malfunction.

To generate a triggering signal for the camera, low- and high-level MCU output was used. For this method, the critical requirement is that sufficient voltage be generated at a specific time. If the camera cannot be triggered at a specific time of orientation, a 3D image could not be generated.

3.3.4.2 MCU trigger

Using the MCU applied in this research, a camera hardware trigger signal was generated using a series of I/O ports (AtMega128). Using the ports of the MCU, a sufficient input of 5 V can be created to trigger the camera. The trigger generation was precisely controlled through embedded code written in C. After the rotation of the stepping motor, the camera trigger signal was set to be generated. Considering the oscillation of the stepping motor, a sufficient time delay was given.

3.3.5 Active shutter glasses

Active 3D is applied to perceive 3D images through a 3D stereoscopic system. Normal active shutter glasses consist of a pair of liquid crystals that control the image detected by the human eye. Alternating blinking of the liquid crystals enables 3D perception. The synchronization of the flickering frequency of the active shutter glasses and the refresh frequency of the image display system play a critical role and thus need to be carefully controlled.

Conventional active shutter glasses (SSG-5100GB, Samsung) were modified for use in this study. The conventional glasses were specially manufactured to be compatible with 3D television using wireless communication at radio frequencies. Two necessary pieces of information about the glasses were not provided: (1) a circuit diagram and (2) the communication standards they used. Without this essential information, slight adjustments of the glasses were impossible, so the original circuit had to be completely removed. Using only the liquid crystal glasses from the conventional glasses, active shutter glasses with modified wiring were created.

The modified 3D glasses were composed only of liquid crystals, a key component of 3D image displays. Because of the electrical properties of the liquid crystal, two factors were experimentally tested for its application: the frequency response and input voltage–transparency relationship.

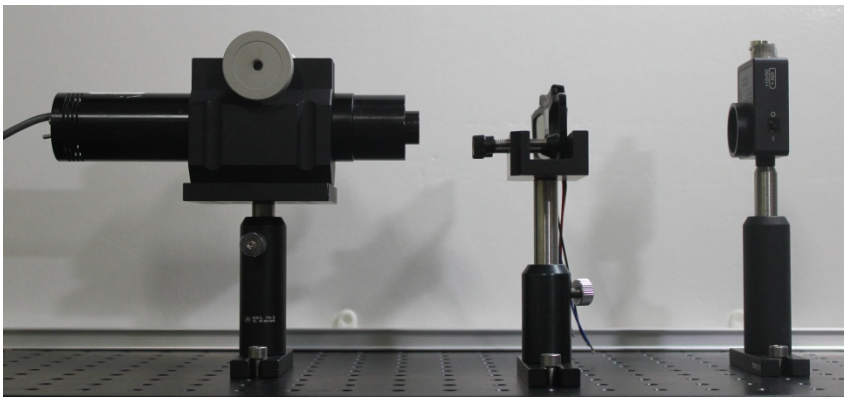

Figure 14. Setup for analysis of active shutter glasses

Using a laser source (10 mW, 633 nm, 1126P, JDS Uniphase), its power supply (1202-2, JDS Uniphase), and a photodetector (DET 36A/M, Thorlab) the properties of the active shutter 3D glasses consisting of liquid crystal glasses were tested, as illustrated in figure 14. The input signal was created using a function generator (DS340, Stanford Research Systems) as an ideal source electrical signal. Both the input frequency and voltage response of the 3D active shutter glasses were tested. The laser was fixed in position, and the frequency response and transparency of the glasses were tested by controlling the input signal of the active shutter. For visual analysis of the input and output waveforms, an oscilloscope (WaveSurfer432, Lecroy) was used, and the waveform results were captured for further analysis. The modified glasses are shown in figure 15.

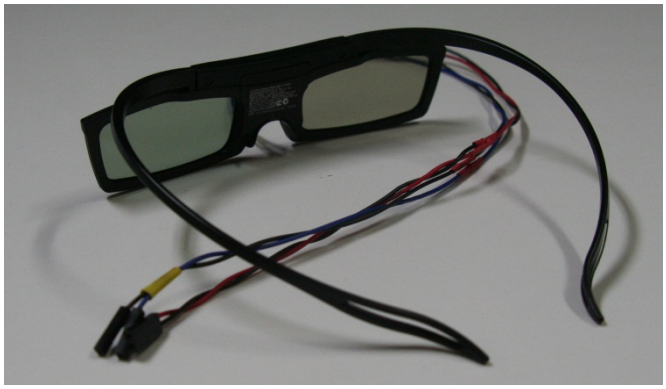

Figure 15. Modified active shutter glasses

3.3.6 3D Display

By using a personal computer (PC, Intel® Core™2 Quad Q9450 @2.66 GHz), the acquired images were displayed on a 3D display monitor (LCD Monitor CM22WS, Samsung). On the basis of the acquired 2D images, a display method was adapted to the system to visualize 3D images. Among many possible visualization methods, the active shutter display method was selected for this application. Theoretically, an alternative method for 3D image visualization could be adopted; however, other methods were not considered owing to their various disadvantages and limited application.

For efficient control, the MCU was used as the signal generator controlling the polarization of the active shutter glasses. Furthermore, a transistor (2N222A) was used as an electrical switch to change the voltage according to the MCU control signal. For this research, the frequency of the monitor had to be manually adjusted depending on the image acquisition rate of the object. The display frequency has to be a constant multiple of the image frame rate in order to properly view 3D images without distortion.

3.4 System Evaluation

3.4.1 System temperature test

As the result of the heat generated by the motor as it rotated, the motor was heated in proportion to the duration of operation. Heat generation in the system components was visually confirmed by imaging using a thermographic camera (CS620, FLIR Systems). The surface temperature of both the stepping motor and the stepping motor driver was measured every 10 min for 150 min using an infrared thermometer (DT8380, Cheerman). It was assumed that if a significant temperature change occurred during system operation, it can be expected to cause the entire system to malfunction. To limit the possible heat generation, a heat reduction system (HRS) using a heat sink and motor fan (CT-6015L05B-2P, COOLERTEC) was devised (figure 16). The heat sink for the motor holder was made from aluminum because of its high thermal conductivity and was mounted on the base plate. The temperature experiment was performed for the system with and without the HRS.

(a) (b)

Figure 16. Heat reduction system: (a) motor fan (CT-6015L05B-2P, COOLERTEC), (b) manufactured heat sink, motor holder (silver), and motor mount (black)

3.4.2 Image property test

Using a reflectance target (figure 17, SRT-99-100, Labsphere) and the previously developed imaging system (figure 18), the image properties at various rotation angles were examined. Images were taken with both left and right rotation of the TRD from 0° to 40°. All the images were taken at ISO-800, an exposure time of 1/125 s, and f/5.6.

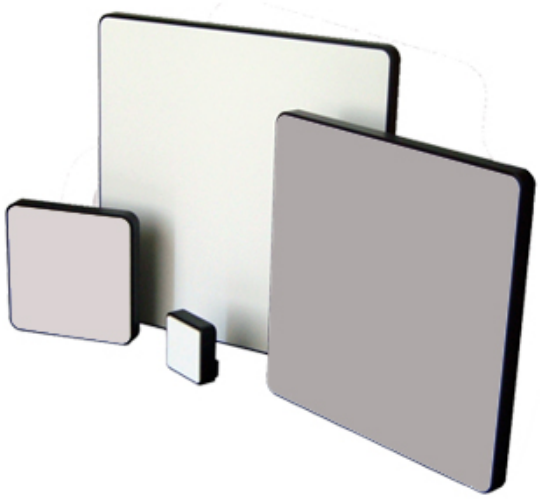

Figure 17. White reflectance target (SRT-99-100, Labsphere)

The coefficients of variation (CVs) of the images were calculated using equation 3. Images taken at different rotation angles were calculated using MATLAB (MathWorks). It was assumed that at a fixed system setting, the CV would be constant; however, any changes in the CV were expected to be influenced by the experimental variable, i.e., the rotation angle.

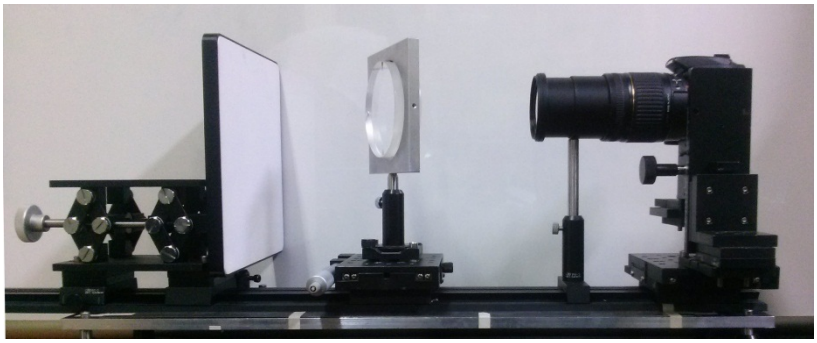

Figure 18. Image property testing system consisting of white reflectance traget, TRD, and DSLR camera

4. Results

4.1 System Simulation

Assuming that image disparity (ID) would be created when light was refracted though the transparent rotating deflector (TRD), light ray propagation and the objective ID were simulated. A light propagation simulation using ZEMAX was performed using BK7 (n = 1.52 at λ = 589 nm) with a thickness of 30 mm. Figure 19 shows a top view of the ID through the TRD. The lateral displacement of light rays differed in proportion to the rotation angle: the larger the rotation angle, the larger the ID. On the basis of the simulation results, it was concluded that the ID depended on the rotation angle of the TRD.

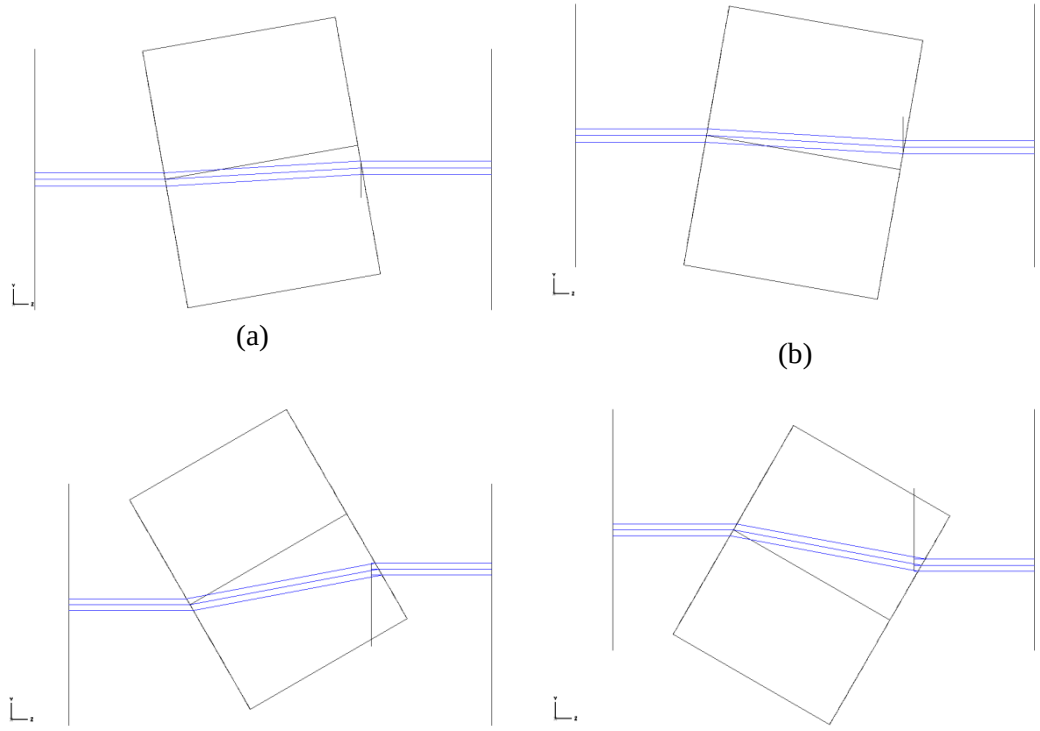

(a) (b)

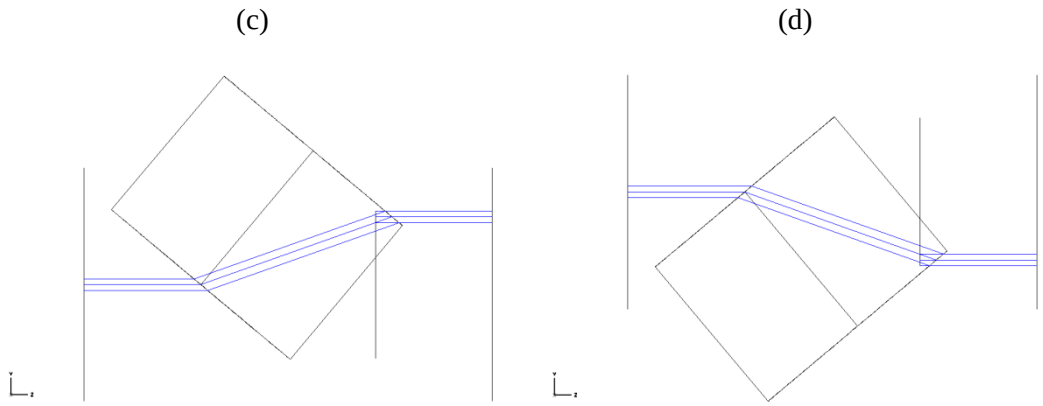

Figure 19. ZEMAX simulation of image disparity for different rotational directions and degrees: (a) 10°L, (b) 10°R, (c) 30°L, (d) 30°R, (e) 50°L, (f) 50°R

For a detailed analysis of the ID, acryl, BK7, and diamond were used, with refractive indices of n = 1.49, n = 1.52, and n = 2.42, respectively, at λ = 589 nm. The surface boundary was assumed to be perfectly flat, and internal reflection was neglected in the simulation. Figure 20 shows a scatter chart based on the simulated ID using acryl, BK7, and diamond. The ID increased as the rotation angle, refractive index, and thickness of the TRD increased. With increasing refractive index, the ID became more linear.

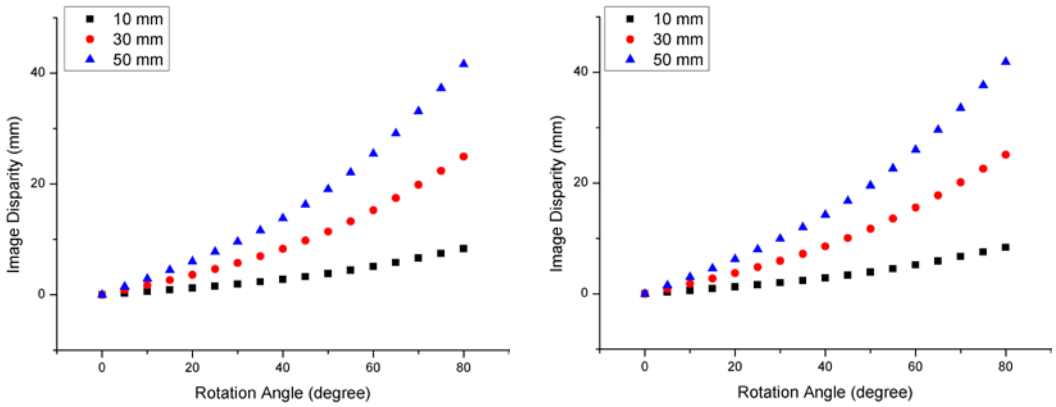

(a) (b)

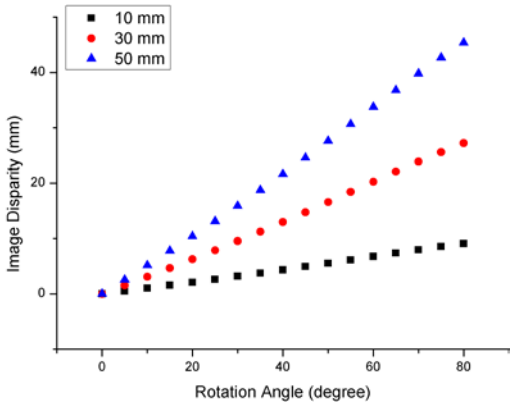

(c)

Figure 20. Image disparity simulation using different materials, rotation angles, and thicknesses: (a) acryl (n = 1.49, λ = 589.29 nm), (b) BK7 (n = 1.52, λ = 589.29 nm), (c) diamond (n = 2.42, λ = 589.29 nm)

4.2 Image Disparity Experiment

The theoretical data were calculated using Snell's law. The theoretical and experimental ID data for the 30 mm thick acryl plate were compared. The experiment was repeated five times for each experimental setup, and the averages and standard deviations were plotted in a scatter chart. Figure 21 shows that the theoretical and experimental data showed a similar pattern. The measured values matched the calculated values well at small rotation angles, and the difference between them increased at higher rotation angles. The ID was constant regardless of the working distance and rotation direction.

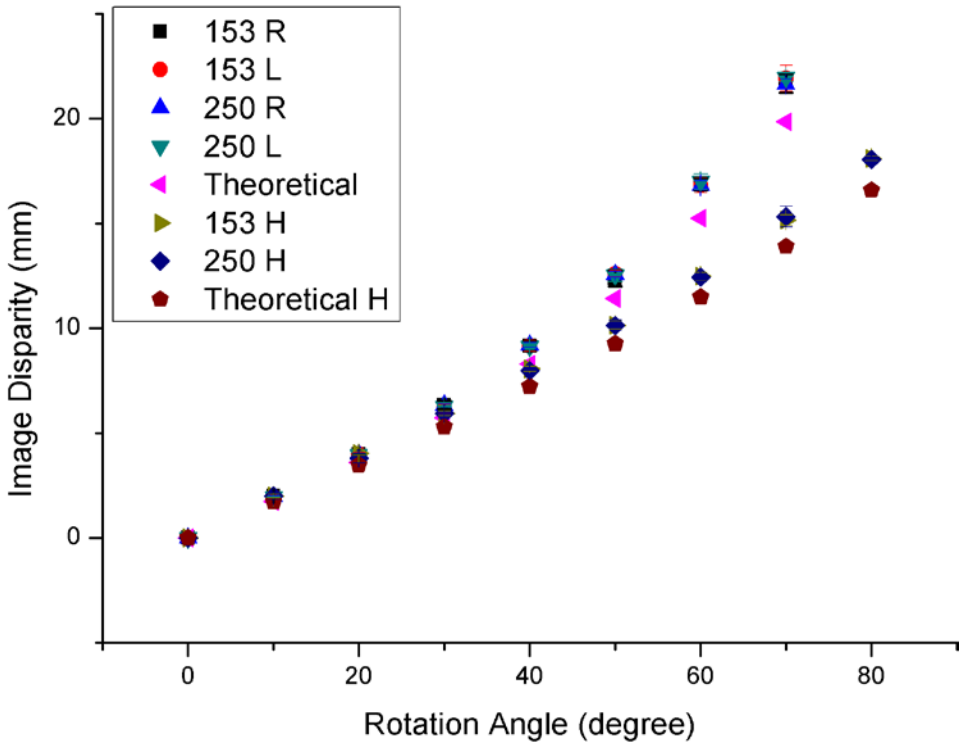

Figure 21. Image disparity versus TRD rotation angle

Figure 22 shows pairs of images taken at 20°H, 60°H, and 100°H. As predicted by the ID simulation, the ID increased with increasing rotation angle. Anaglyphs of the left and right images were created to visualize the ID, which was greater at 100° H than at 20°H and 60°H. The experimental data seem to correspond well to the calculated data.

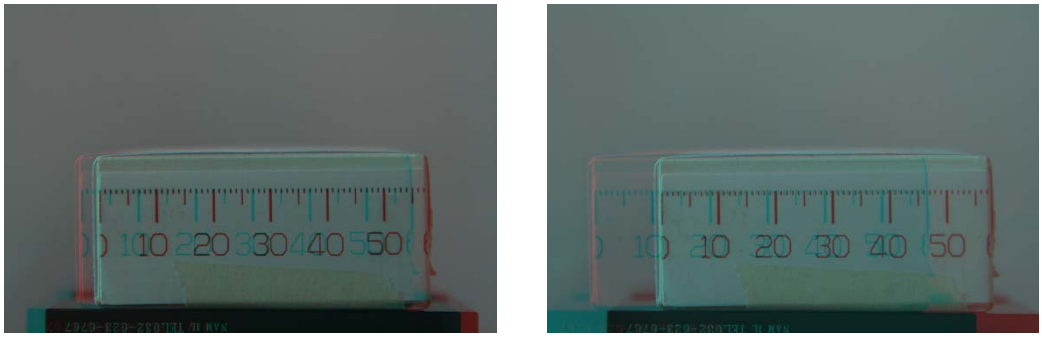

(a) (b)

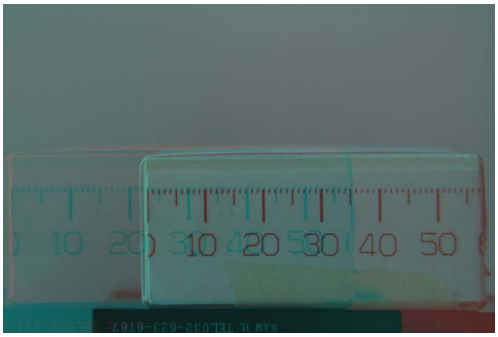

(c)

Figure 22. Anaglyph of left and right images taken at rotation angles of (a) 20°H, (b) 60°H, and (c) 100°H

4.3 Real-time 3D Imaging System

Figure 23 depicts a new concept for 3D imaging based on single-channel optics. The optical system is composed of a camera and a TRD. For real-time imaging, the transparent deflector is mounted on a stepping motor. The image detected by the camera is displayed using a computer. To display 3D images from 2D images, an active 3D method was adopted. Active shutter glasses were created using liquid crystals. Conventional 3D active shutter glasses were modified for this research purpose, as described in section 3.3.5.

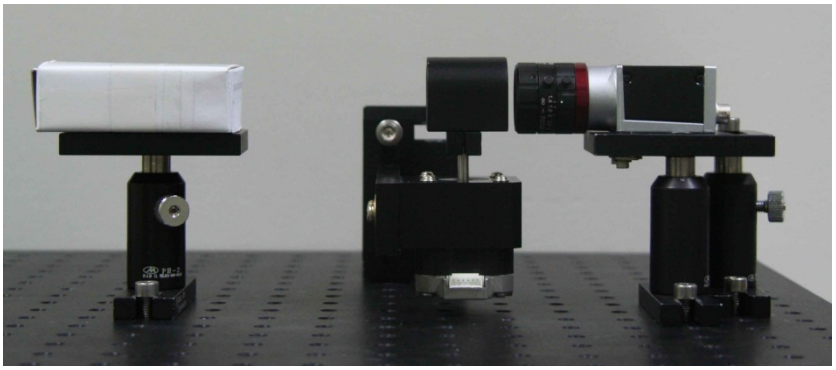

Figure 23. Real-time TRD-based stereoscopic imaging system (RT-TRD-SIS)

4.3.1 Rotation method

4.3.1.1 Galvanometer

The stability and repeatability of the galvanometer were tested using an optical setup in figure 23. The reflected laser was detected while the input signal was varied. Figure 24 shows the repeatability of the laser reflection from the galvanometer. As the results show, the detected intensity was constant regardless of the input frequency.

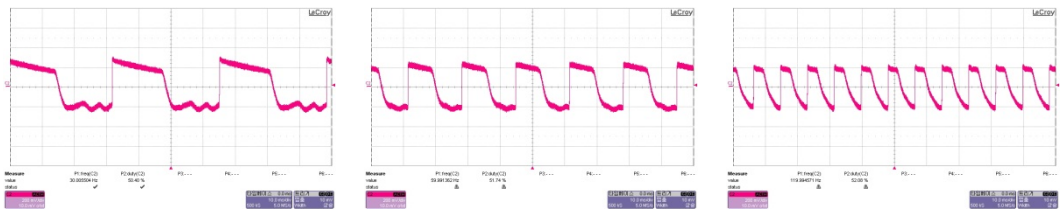

(a) (b) (c)

Figure 24. Detection of laser reflection from galvanometer:

(a) 30 Hz, 50% duty rate, (b) 60 Hz, 50% duty rate, (c) 120 Hz, 50% duty rate

To create an ID with the galvanometer, it was suggested that the optical mirror be replaced with a transparent optical window. Considering the mechanical specifications of

the current optical mirror, a thin transparent optical window of BK7 was manufactured with a diameter of 20 mm, thickness of 1.73 mm, and mass of 1.33 g, as shown in figure 25.

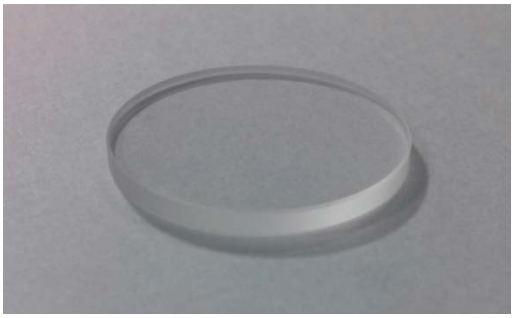

Figure 25. Transparent optical window

The ID was examined using the modified galvanometer. However, because of the mirror's thinness, the ID was not noticeable. A calculation confirmed that a TRD 1.73 mm in thickness would create an ID of only 0.43 mm at 40°H. Even though the galvanometer was suitable for generating an ID, the deflected light was very limited owing to its thickness.

If the thickness of the manufactured TRD were increased, its mass would increase accordingly. A galvanometer can function only within its specified fixed rotor inertia and constant torque. Increasing the size of the TRD would change its effect on the galvanometer, thus possibly exceeding the mechanical specifications. Exceeding these limits may cause the galvanometer to malfunction and produce unstable rotation of the optical window. Therefore, the galvanometer was excluded from the setup, and a different method of rotation was necessary.

4.3.1.2 Stepping motor

For this research, a unipolar stepping motor and a unipolar stepping motor driver were selected. A typical unipolar stepping motor has a rotation angle of 1.8° per clock cycle. The stepping motor was controlled for continuous and rapid movement. It was controlled to provide rotation of up to 25 rotation cycles, which ultimately yielded 25 pairs of left and right images.

However, at 25 rotation cycles, oscillation before the motor stop due to the characteristics of the stepping motor was detected. Consequently, image acquisition during oscillation is expected to cause image distortion. At small rotation cycles, the oscillation may be reduced; however, the final 3D images may have low frame rates.

4.3.2 Transparent rotating deflector (TRD) and TRD mount

On the basis of the results of the ID experiment, a TRD and matching TRD mount were manufactured. They were designed to create an ID while mounted on the stepping motor axis. Figure 26 shows the design.

The TRD was designed in a cylindrical shape 30 mm in thickness and 25 mm in diameter. It was designed to be large enough to cover marginal rays from the CMOS camera lens. The designed lens weighed approximately 37.53 g. To mount the manufactured TRD on the stepping motor, a TRD mount was devised to fix the TRD in place while it was continuously rotated by the motor. The TRD was placed inside the mount and held in place by a retainer ring. The mount was made of aluminum and anodized to prevent oxidization of the aluminum. The final mount had a mass of 39.78 g and weighed a total of 77.31 g when the TRD was inserted.

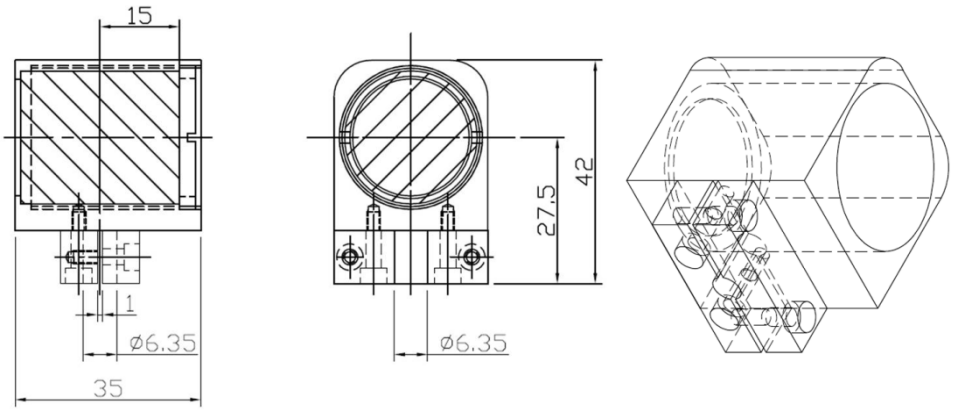

Figure 26. TRD mount design drawing

4.3.3 Active shutter glasses

4.3.3.1 Frequency response

The obtained frequency response of the 3D active shutter proved its potential for application in 3D imaging. Four frequencies were tested for a thorough verification: 24 Hz, 30 Hz, 60 Hz, and 120 Hz.

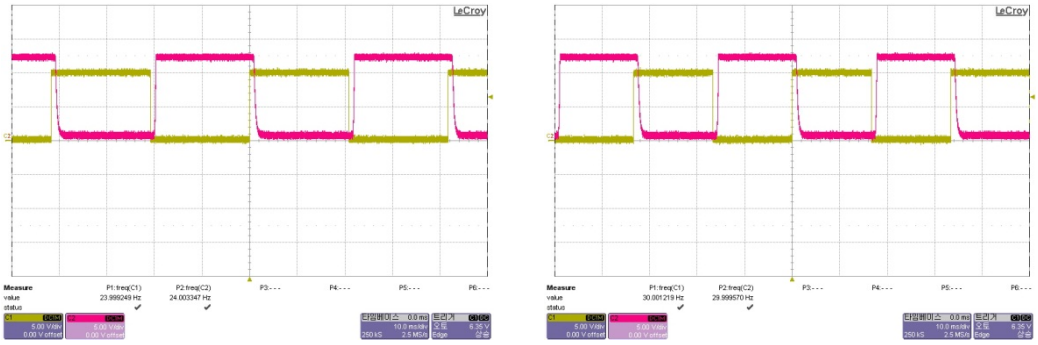

(a) (b)

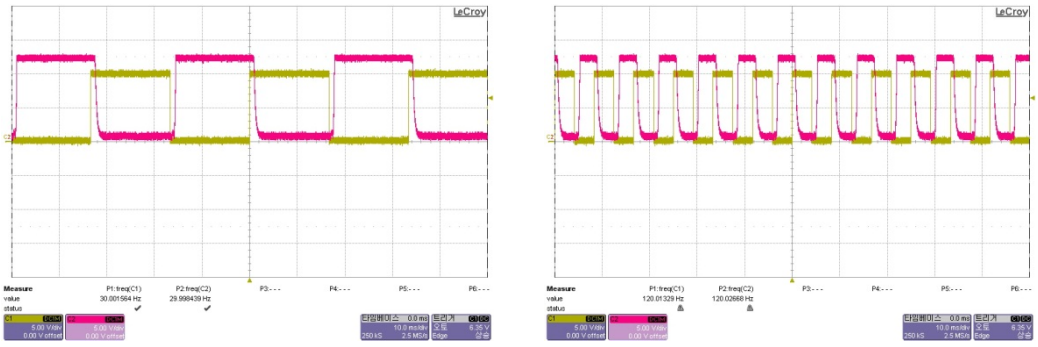

(c) (d)

Figure 27. Frequency response of 3D active shutter glasses. Channel 1 (yellow): input voltage signal, channel 2 (pink): active shutter glasses transparency. (a) 24 Hz, (b) 30 Hz, (c) 60 Hz, (d) 120 Hz

Figure 27 shows images captured by the oscilloscope that compare the 3D active shutter glasses input control signal and the intensity of the light detected after it penetrated the 3D active shutter glasses. Channel 1 represents the input control signal of the active 3D glasses, and channel 2 represents the light intensity detected at the photodetector.

The 3D active shutter glasses showed good follow-up; however, some delay between channels 1 and 2 was noticed. A time delay of approximately 2 ms was noticed as the transparency changed; however, it was independent of the input control frequency.

4.3.3.2 Voltage response

As the input signal of the liquid crystal was adjusted, the intensity of the penetrating light varied accordingly. As the voltage of the input signal increased, the transparency of the liquid crystal decreased in relation to the input, as shown in figure 28. However, as

the input voltage increased above a certain level, the transparency was already maximized, eliminating any further need for higher input voltages.

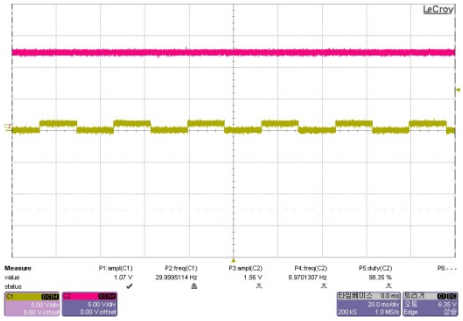

(a)

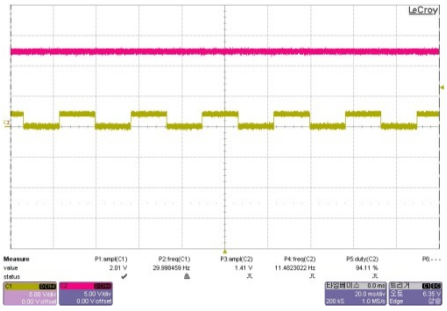

(b)

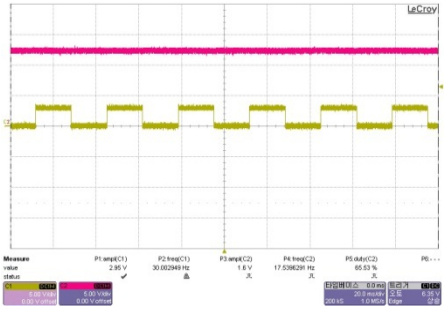

(c)

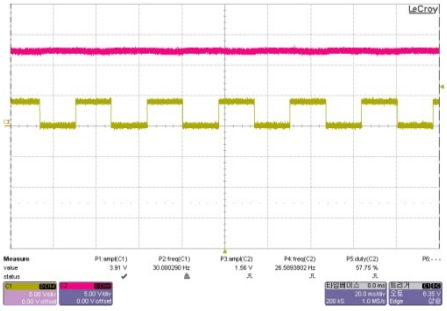

(d)

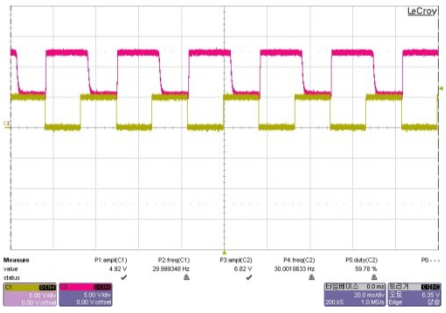

(e)

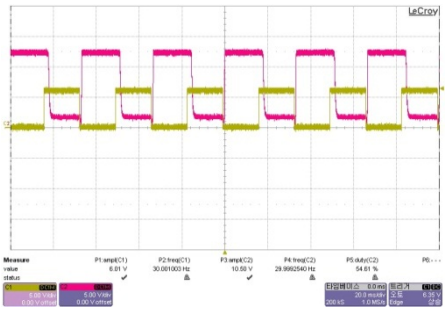

(f)

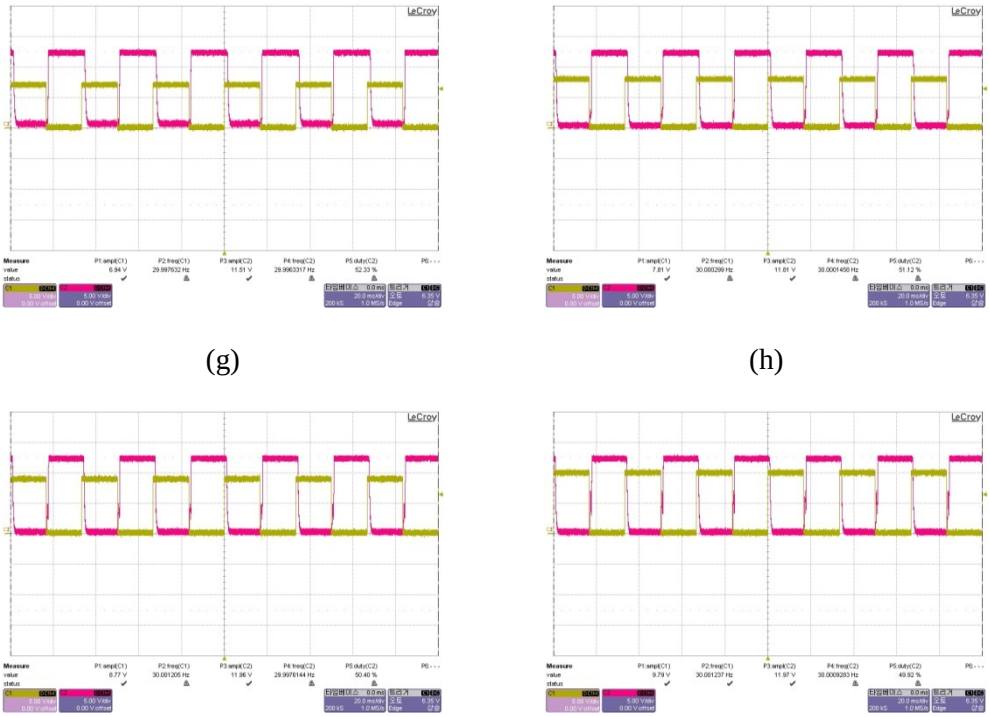

(g) (h)

(i) (j)

Figure 28. Voltage–transparency relation (0–10 V)

4.3.4 3D Display

The acquired images were displayed in real time using a computer and display monitor. For the system developed here, the image acquisition frame rate was set to 50 fps, so it acquired 50 images per second. The frequency of the display system was set to 100 Hz, a constant multiple of the image frame rate, as previously stated.

4.4 Acquired 3D Images

By using a TRD spectroscopic imaging system (SIS) and real-time TRD-SIS (RT-TRD-SIS), 3D images were acquired and displayed on a computer monitor. Different targets were used to experimentally test the feasibility. To clearly show the ID generated

in both systems, anaglyphs were created in which the left and right images were overlapped, as shown in figures 29–32. Red–cyan glasses should be worn to perceive a 3D image.

(a)

(b)

(c)

Figure 29. Sample stereoscopic image from TRD-SIS: (a) left image (10°, 0°) (b) right image (0°, 10°), (c) anaglyph (10°, 10°)

(a)

(b)

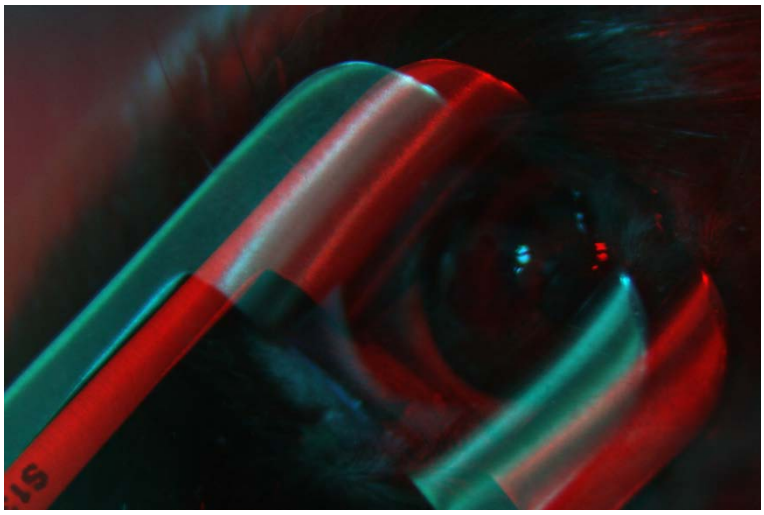

(c)

Figure 30. Sample stereoscopic image from TRD-SIS: (a) left image (20°, 0°), (b) right image (0°, 20°), (c) anaglyph (20°, 20°)

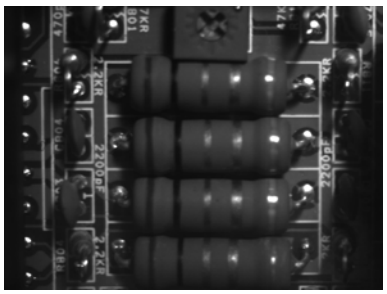

(a)

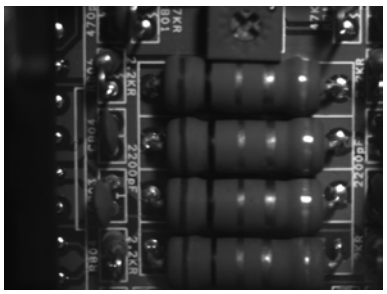

(b)

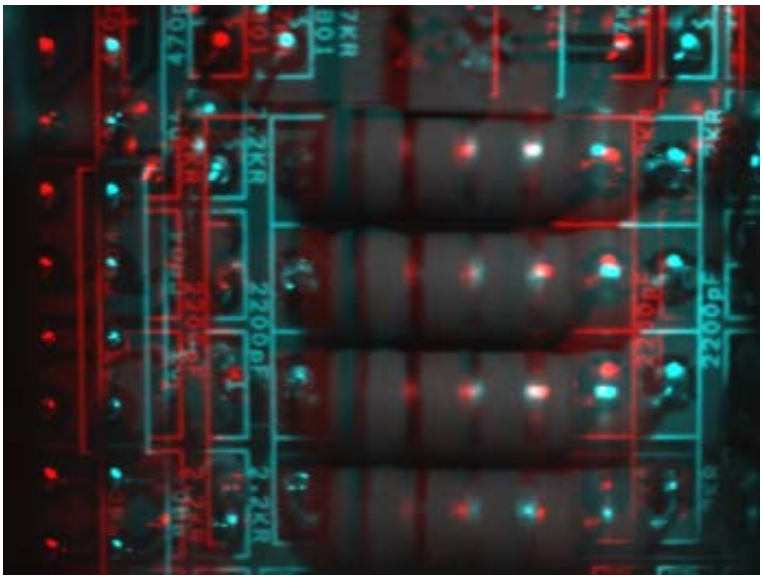

(c)

Figure 31. Sample stereoscopic image of hardware circuit obtained using RT-TRD-SIS:

(a) left image (9.9°, 0°), (b) right image (0°, 9.9°), (c) anaglyph (9.9°, 9.9°)

(a)

(b)

(c)

Figure 32. Sample stereoscopic image of hexagonal wrench handle obtained using RT-TRD-SIS: (a) left image (9.9°, 0°), (b) right image (0°, 9.9°), (c) anaglyph (9.9°, 9.9°)

4.5 Modularization

For convenient use of the control system, the MCU, motor driver, and hardware circuit were fixed in a box. The module box was fabricated using aluminum and was anodized to prevent further oxidization at the metal surface. An open window and motorized fan were added to allow airflow through the module. The components were fixed at the bottom, and a hole for wiring was drilled on the side. The resulting setup is shown in figure 33.

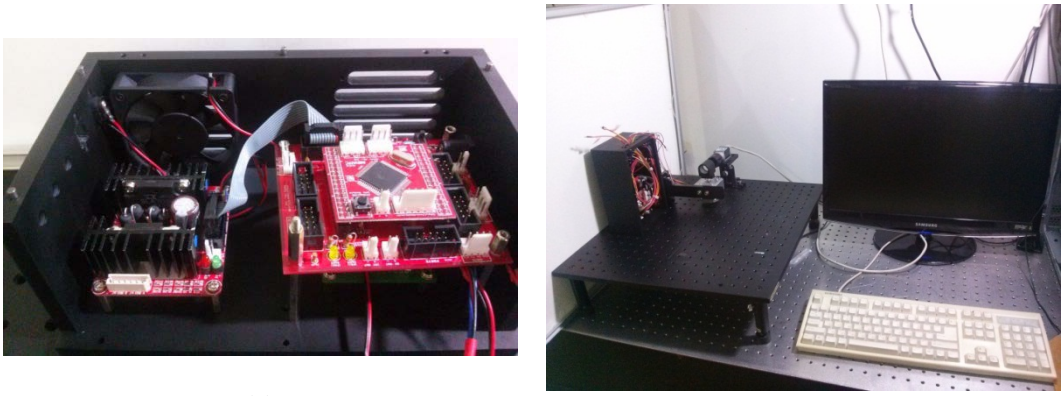

(a) (b)

Figure 33. Devised single-channel stereoscopic imaging system: (a) modularized control system box, (b) entire system setup with PC monitor

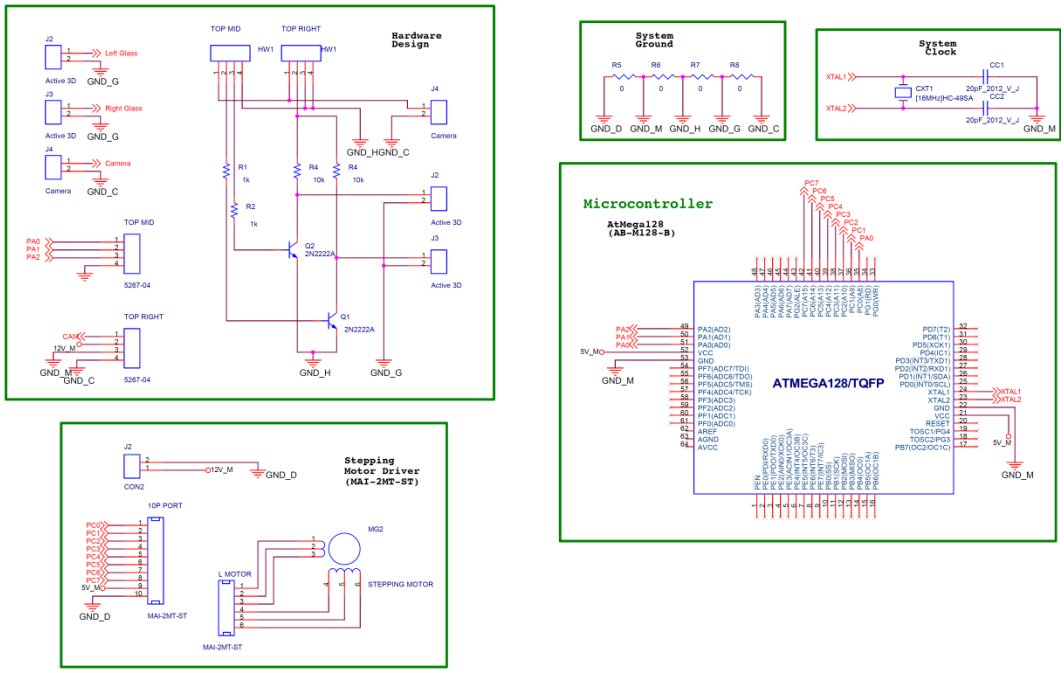

Figure 34. Hardware circuit design showing connection schematic of MCU, motor, motor driver, and active shutter glasses

The internal connections of the final hardware system are shown in figure 34. Among the many general-purpose input/output (GPIO) ports, PORTB was connected to the motor driver, which controls the connected stepping motor. To obtain sufficient power input, a separate electrical adaptor was connected to act as the motor driver. To control the polarization of the liquid crystals in the active shutter glasses, 12 V was generated and connected to the glasses. The GPIO can produce 5 V at a high-level output, which is sufficient to control a transistor. Using PORTA, the 2N2222A transistor was controlled as an electrical switch to switch the 12 V input connected to the active shutter glasses. The hardware camera trigger was also generated using PORTA, and all the grounds were connected with each other.

4.6 System Evaluation

4.6.1 System temperature test

The temperatures of both the stepping motor and the stepping motor driver rose in proportion to the duration of operation. The surface temperature was measured in experimental setups with and without a heat reduction system (HRS). Each experiment was repeated six times; using the experimental data, line-scatter charts were plotted using the averages and standard deviations for 150 min of operation.

As shown in figure 35, the temperature of the system components increased with increasing time at the motor and motor driver. In 150 min of operation, the temperature at the motor (black) and the driver (turquoise) without the HRS increased to 82°C and 45°C, respectively. Both system components showed similar patterns in which the temperature exhibited a dramatic rapid increase followed by a slow steady increase.

When the HRS was used, the heat generation was limited, although the pattern was similar to that of the experimental data acquired without the HRS. After 150 min of operation, heat generation was limited to 41°C and 26°C at the motor and driver, respectively, showing a slower increase in temperature.

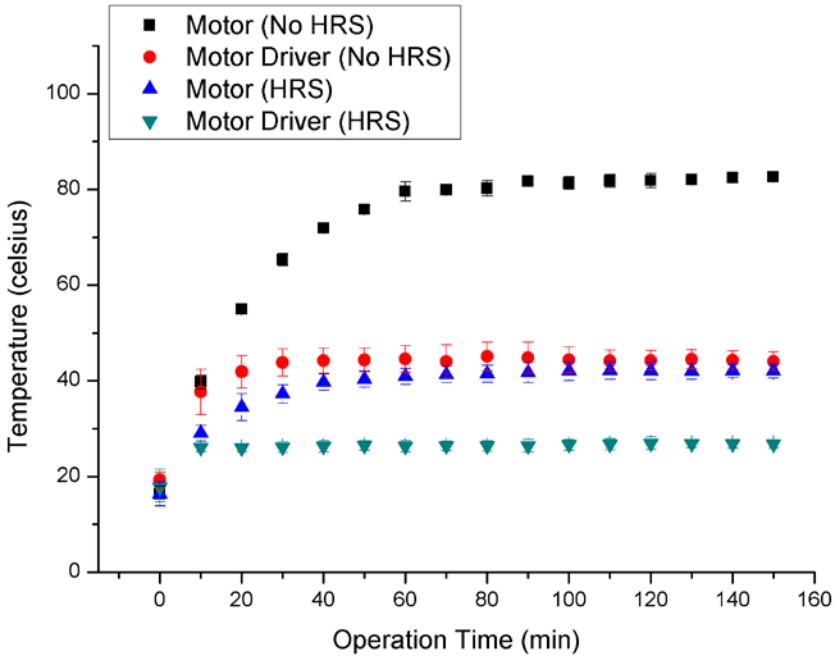

Figure 35. Heat generation at the motor and driver during 150 min of operation

The heat generation was visually confirmed using a thermocamera during 150 min of operation. As shown in figure 36, most of the heat was generated at the stepping motor and motor driver. The SLA7062M, a critical component of the motor driver, showed the most heat generation among the hardware components. Slight heating was noticed at the CMOS camera throughout operation of the system; however, such temperature change was neglected since it is expected to have minor impact on the overall system.

The aluminum motor holder and mount acted as a heat sink and efficiently removed the generated heat, limiting the temperature increase at the holder. However, when the motor mount lacked a heat sink, the heat increased continuously.

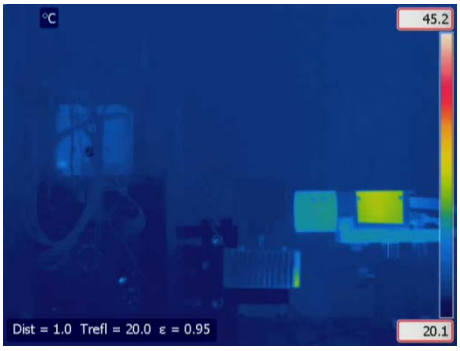

(a)

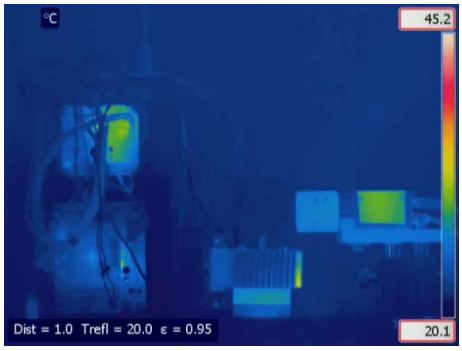

(b)

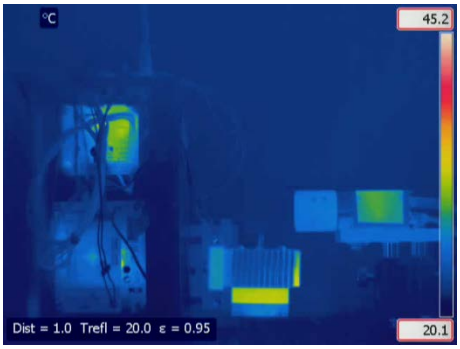

(c)

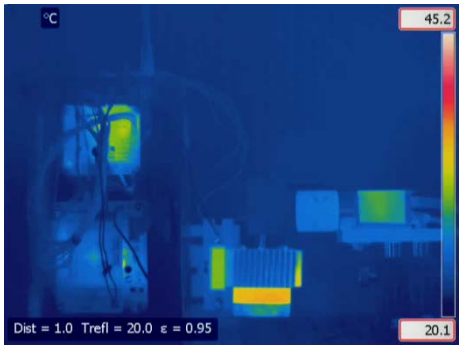

(d)

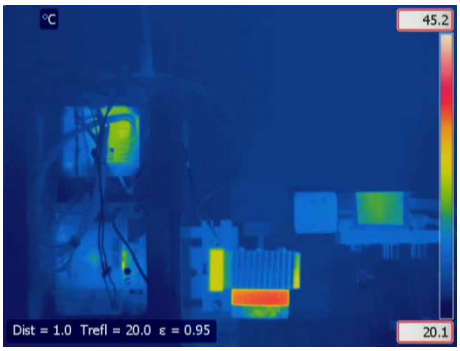

(e)

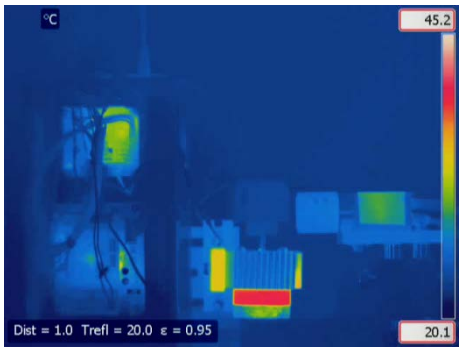

(f)

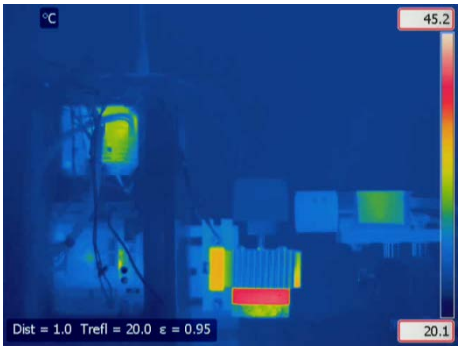

(g)

Figure 36. Thermocamera images of automated system with HRS during 30 min of operation: (a) 0 min, (b) 5 min, (c) 10 min, (d) 15 min, (e) 20 min, (f) 25 min, (g) 30 min

4.6.2 Image property test

The coefficients of variation (CVs) of the acquired images were calculated and plotted for an objective analysis. Because the imaging system lacked a light source, the experiment was conducted in a natural light environment. The experiment was repeated 11 times; the averages and standard deviations were calculated, and line-scatter charts were plotted for comparison. The average CV was 3.3% and was independent of the rotation angle of the TRD (figure 37). A slight difference was detected at a rotation of 30°; however, this difference was an experimental error caused by working in a natural environment. Therefore, it was concluded that the CV was independent of the rotation angle of the TRD.

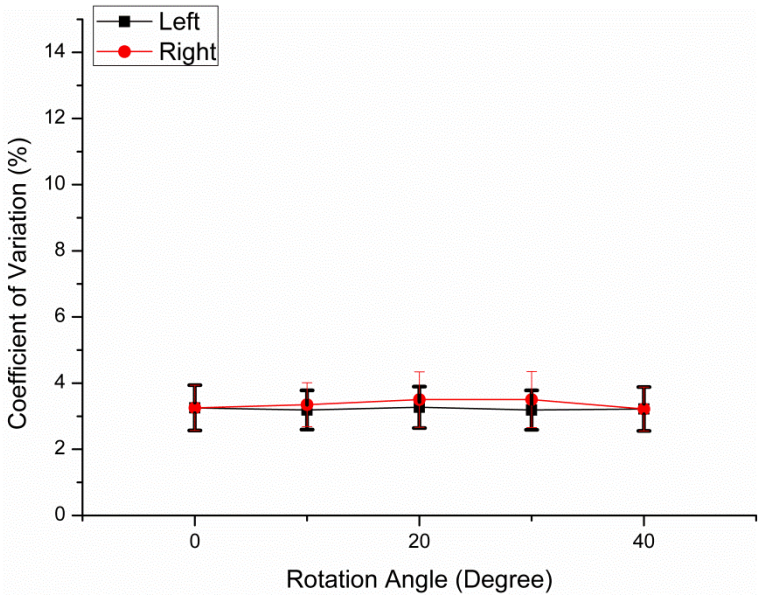

Figure 37. Coefficient of variation versus rotation angle

5. Discussion

According to previous studies, the single-channel stereoscopic system has several advantages over the conventional dual-channel stereoscopic system: 1) simple manipulation of the magnification, focus, and exposure time with a single channel; 2) complete synchronization of right and left images; 3) identical geometrical matching (no rotational error, no size difference, and no vertical/horizontal shift) between the left and right images; and 4) identical image characteristic matching (color, white balance, and brightness).

As shown in figure 21, the image disparity (ID) was proportional to the rotation angle. However, the results in figure 20(a) and (b) showed a slightly different pattern of increase compared to that in figure 20(c). In figure 20(a) and (b), the ID seemed to increase exponentially, but in figure 20(c), it seemed to increase more linearly. As shown in figure 6, line $\overline{BC}$ depends on angle $\angle$FOC, which is affected by the refractive index (n) of the transparent rotating deflector (TRD). Diamond has a higher refractive index (n = 2.42) than acryl and BK7, so it causes greater refraction, resulting in greater ID. When the refractive index is high, line $\overline{OC}$ is similar to line $\overline{OF}$, which creates a large ID. If a material with an even higher refractive index is used, the ID versus the rotation angle would be more linear.

The measured values showed a trend similar to that of the theoretical ID values. However, the difference seemed to increase as the rotation of the TRD increased. This phenomenon may be explained by the fact that the assumptions made for the calculated values did not totally agree with the conditions for the experimental measurements. For

instance, the inner layers within the acrylic plate may have played a role, causing an index mismatch between the layers of the TRD. In addition, the surface of the TRD may not be perfectly flat, causing the difference between the theoretical and experimental values to increase with increasing TRD rotation angle.

On the basis of the simulated and experimental results, it was concluded that ID can be generated by rotating the TRD. The ID increased as a function of the rotation angle. The ID was also tested under different working distances; however, the results did not vary owing to the parallel displacement of the image rays, as described in figure 6 and equation 2.

Although this study investigated the ID only as a function of the TRD angle, the ID can be also affected by the thickness and material of the TRD. Therefore, various other factors must be considered and characterized to improve the image quality in future studies. In this study, the TRD was designed to be large enough to cover the camera lens. However, depending on the location of the TRD, its size can be greatly reduced. If the TRD is located between the optical lenses, its size could be reduced accordingly.

Because humans have two eyes, the ID of a target is processed in the brain, and a final 3D image is recognized. The ID and angle of convergence play a critical role in both the depth of 3D images and the location of 3D image scenes.(Mendiburu 2009) When the axes of the cameras are parallel, the final 3D image is normally in front of the display screen; furthermore, with increasing ID, the depth between the near plane and far plane of 3D images is proportionally increased. However, when the axes of the cameras converge at a point, the converged point is often recognized as being at the 3D display screen.

However, in this research the image rays are parallel to each other, placing the generated 3D image in front of the screen. For applications where the location of the 3D

image is critical, the developed system may not be applicable; however, it may be possible to devise a method of converging the image rays in the system.

The frequency response of the 3D active shutter glasses was shown to be well matched up to 120 Hz. To perceive a continuous image, a minimal refresh frequency has to be satisfied. This frequency may vary slightly from person to person, but it is generally assumed to be 24 Hz.

Because the workload on a single camera was twice that in a conventional dual-camera stereoscopic imaging system, the camera requires a high frame rate. According to the literature, many types of camera sensors are available for imaging, and each sensor type has a different structure.(Hain, Kähler, and Tropea 2007, 403-411) A CMOS sensor provides an adequate frame rate because of its high internal processing speed, which was a critical factor in this imaging system. However, it tends to have larger pixels than a CCD camera; however, with constant developments in semiconductor technology, such limitations are expected to be eliminated.(Carlson 2002, 171-176 vol.1)

At a high frame rate, the amount of image information that needs to be transferred and received increases proportionally. Several data interface methods exist, including camera link, FireWire, GigE Vision, and USB. Each has advantages and disadvantages over the others; however, the currently used GigE Vision interface is known to have several advantages, such as no or low cost for frame grabbing, a long image transfer distance, and high bandwidth for real-time imaging. With these advantages, real-time 3D imaging was possible at sufficient resolution. However, because of its characteristics, GigE Vision provides limited bandwidth compared with the camera link interface, and it has a high

CPU load at the connected PC. For a higher frame rate, a camera link seems to be the solution.

The current stepping motor has a step angle of 1.8°, so it has a fixed rotation angle that is a constant multiple of the step angle. Some stepping motors provide half-stepping or microstepping functions that allow a smaller step angle. Using such functions, the rotation becomes smoother, and this may reduce the oscillation or resonance at the motor or parts connected to the motor. These functions may be applied to the current research system to reduce the oscillation at the stepping motor, allowing image acquisition with less error.

The delay in the motor rotation can be removed by either limiting the rotation angle of the TRD or using a different rotation method that has sufficient motor power. When the rotation angle of the TRD is limited, the final 3D image may look farther away compared to the image plane. On the other hand, when the TRD rotation angle is increased, the image will appear closer. This behavior will be eliminated when a bigger motor with greater rotation power is used, but the physical size of the motor could increase, making the 3D imaging system bulky.

As stated in the specifications for the stepping motor used here, the insulation was a class-B type, which has a maximum operating temperature of 130°C. Most of the heat in the motor driver was generated from the SLA7062M component, a unipolar stepping motor translator. As stated in the specification sheet, the operating temperature ranges between -20°C and +85°C. Fortunately, in 150 min of operation, the temperature of both the motor and the motor driver did not exceed the recommended operating temperature.

However, long-duration operation of several hours can be expected for the imaging system. In the future, an experiment with a longer operation time is needed to analyze the heat reduction during operation. On the basis of the current experimental results, which showed a slow steady increase in temperature, it can be assumed that the temperature may reach maximum operating temperature after several hours. For even longer operation, a better HRS may be required.

In this research, a stepping motor was used to rotate the TRD. Owing to its operation method, vibration is inevitable. The sudden rotation during motor steps creates oscillation of the motor's status even at a single point. The degree of oscillation depends on the rotation speed of the stepping motor, with more oscillation at higher speeds and less oscillation at lower speeds. The oscillation is expected to stop after a certain time; however, the time varies greatly depending on the weight of the mounted object and the mechanical specifications of the stepping motor.

As the sample images show, image distortions due to motor oscillation affected the quality of the acquired images. Because of the oscillation of the stepping motor, the image acquired at the trigger was usually unfocused or distorted. At a slow rotation speed, no image distortion was noticed, but at higher rotation speeds, the image distortion was pronounced. For practical application of the system, it should be adjusted to eliminate oscillation during TRD rotation. A possible solution for these problems is replacement of the stepping motor. A DC motor or servo motor is known to be applicable in systems that require high speed with less oscillation.

The final 3D image was obtained using 3D active shutter glasses and a 3D image display monitor. The proposed system can display a 3D image at 25 fps owing to several factors: a delay in the image display due to the time consumed during image acquisition, a delay due to motor rotation, the monitor refresh rate, and the refresh frequency, which is limited by the image acquisition software.

The display monitor used here, like most computers, has a fixed number of display frequency settings. To display an ideal 3D image, the frequency of the monitor must match or be a constant multiple of the frame rate during image acquisition. A frequency mismatch could cause image distortion, and possibly no 3D image could be detected. Furthermore, the image acquisition software used in this research has a limit of 50 fps, allowing only 25 fps to be detected in each eye. A 25 fps 3D image will appear continuous; however, owing to the blinking of the 3D active shutter glasses, the detected image may look darker than usual.

To eliminate the limitations imposed by the image acquisition software, a new program has to be developed that allows live streaming of the acquired images at a higher frame rate. Instead of the currently used LabVIEW (National Instruments), a live image streaming program written in C or C++ could produce better 3D images. In addition, to eliminate the inconvenience of manual adjustment of the refresh rate of the image display monitor, a method of automatic adjustment could ease the difficulty of applying the current research system.

Depending on the application, the rotation angle of the TRD and the exposure time of the camera may need to be altered. Changing such factors could alter the camera frame rate, thus requiring the display frequency to be changed as well. Because a conventional

monitor was used, only a limited set of display frequencies can be used. To use different display frequencies, a monitor that can selectively change the display should be chosen.

The image properties were tested by calculating the coefficient of variation (CV). As expected, the CV was constant regardless of the TRD rotation angle. In this research, the TRD rotation angle was varied between 0° and 40° at 10° intervals. The acquired results show a constant CV regardless of the rotation angle. Because this experiment examined rotation angles of up to 40° for accurate analysis of the imaging system, the TRD should be rotated by higher rotation angles and at smaller intervals. However, the current results suggest that even at higher rotation angles, the CV should be constant.

Because the experiment was performed in a natural environment owing to the lack of a light source, a slight experimental error was observed. When a system module is manufactured, a light source should be designed and tested.

Some discomfort was noticed when the developed system was used to view 3D images. The active 3D glasses and their control components were connected using wire. Because of the connecting wire, the distance between the viewer and the integrated system and its monitor is limited. The distance may be lengthened if a longer connecting wire is used, but this could cause safety issues or system malfunction.

A suggested solution is the adoption of a wireless communication system capable of signal transfer and the generation of a sufficient voltage to control the transparency of the active 3D glasses. In this work, a sufficient voltage flowed through the connecting wire; however, if a wireless connection is used, the actual electrical voltage cannot be

transferred. In this case, the signal-generating triggers can be transferred, and after they are received, a sufficient voltage could be generated.

For practical use of the developed system, the final image should be evaluated in terms of several factors: the image properties, image distortion, and visual fatigue. The image properties and image distortion may be evaluated using software; however, visual fatigue is a physiological factor that cannot be determined objectively but must be evaluated using a survey. The 3D image from the current system may not be an ideal image, so a conventional 3D image display should be used as a benchmark to test the performance.

6. Conclusion

In this study, a single-channel 3D imaging system was designed, and its feasibility was tested. Image disparity (ID) between the left and right images was generated by rotating a transparent rotating deflector (TRD). The generated ID can be adjusted by controlling the rotation angle of the TRD. Using a continuous rotation method, continuous rotation of the TRD was achieved, allowing alternating acquisition of 2D images. Finally, using a method based on active 3D display, the acquired images were viewed in 3D.

This system not only will overcome the limitations of conventional dual-channel 3D imaging systems but may also reduce the size and overall production cost of stereoscopic imaging systems. Because of the limitations on camera specifications, applications in medicine may be challenging, but it could become an economical stereoscopic imaging system.

7. References

[1] Abdi, H. 2010. "Coefficient of variation". Encyclopedia of Research Design. SAGE Publications, Inc., Thousand Oaks, CA: 169-171.

[2] Bendel, R., S. Higgins, J. Teberg and D. Pyke. 1989. "Comparison of skewness coefficient, coefficient of variation, and Gini coefficient as inequality measures within populations". Oecologia, 78(3): 394-400.

[3] Blundell, B. G. and A. J. Schwarz. 2000. Volumetric Three-dimensional Display Systems. John Wiley & Sons, Incorporated. ISBN 9780471239284.

[4] Chan, A. C. W., S. C. S. Chung, A. P. C. Yim, J. Y. W. Lau, E. K. W. Ng and A. K. C. Li. 1997. "Comparison of two-dimensional vs three-dimensional camera systems in laparoscopic surgery". Surgical Endoscopy-Ultrasound and Interventional Techniques, 11(5): 438-440.

[5] Choi, W., V. Rubtsov and C.-J. Kim. 2012. "Miniature Flipping Disk Device for Size Measurement of Objects Through Endoscope". Microelectromechanical Systems, Journal of, 21(4): 926-933.

[6] Cope, D. A. and M. G. Lacy. 1995. "Comparative application of the coefficient of variation and range-based statistics for assessing the taxonomic composition of fossil samples". Journal of Human Evolution, 29(6): 549-576.

[7] Cuschieri, A. 1991. "MINIMAL ACCESS SURGERY AND THE FUTURE OF INTERVENTIONAL LAPAROSCOPY". American Journal of Surgery, 161(3): 404-407.

[8] Dodgson, N. A. 2005. "Autostereoscopic 3D Displays". Computer, 38(8): 31-36.

[9] DooHyun, L. and K. Inso. 2000. "A novel stereo camera system by a biprism". Robotics and Automation, IEEE Transactions on, 16(5): 528-541.

[10] Durrani, A. F. and G. M. Preminger. 1995. "3-DIMENSIONAL VIDEO IMAGING FOR ENDOSCOPIC SURGERY". Computers in Biology and Medicine, 25(2): 237-247.

[11] Goldstein, E. B. 1999. Sensation and perception. Brooks/Cole Pub. ISBN 9780534346805.

[12] Hain, R., C. J. Kähler and C. Tropea. 2007. "Comparison of CCD, CMOS and intensified cameras". Experiments in fluids, 42(3): 403-411.

[13] He, X. and S. O. Oyadiji. 2001. "Application of coefficient of variation in reliability-based mechanical design and manufacture". Journal of Materials Processing Technology, 119(1–3): 374-378.

[14] Hecht, E. 2002. Optics. Addison-Wesley Longman, Incorporated. ISBN 9780805385663.

[15] Hofmeister, J., T. G. Frank, A. Cuschieri and N. J. Wade. 2001. "Perceptual aspects of two-dimensional and stereoscopic display techniques in endoscopic surgery: review and current problems". Semin Laparosc Surg, 8(1): 12-24.

[16] Hong, J., Y. Kim, H.-J. Choi, J. Hahn, J.-H. Park, H. Kim, S.-W. Min, N. Chen and B. Lee. 2011. "Three-dimensional display technologies of recent interest: principles, status, and issues [Invited]". Applied optics, 50(34): H87-H115.

[17] Hutarew, G., K. Moser and O. Dietze. 2004. "Comparison of an auto-stereoscopic display and polarized stereoscopic projection for macroscopic pathology". Journal of telemedicine and telecare, 10(4): 206-213.

[18] McDougall, E. M., J. J. Soble, J. S. Wolf, S. Y. Nakada, O. M. Elashry and R. V. Clayman. 1996. "Comparison of three-dimensional and two-dimensional laparoscopic video systems". Journal of Endourology, 10(4): 371-374.

[19] Mendiburu, B. 2009. 3d Movie Making: Stereoscopic Digital Cinema from Script to Screen. Focal Press/Elsevier. ISBN 9780240811376.

[20] Mitsuhashi, T. 1996. "Evaluation of stereoscopic picture quality with CFF". Ergonomics, 39(11): 1344-1356.

[21] Palovuori, K. and I. Rakkolainen. 2012. "The vanishing display: an autovisible immaterial display". Paper presented at Proceeding of the 16th International Academic MindTrek Conference, at Tampere, Finland.

[22] Qin, Z., K. Wang, F. Chen, X. Luo and S. Liu. 2010. "Analysis of condition for uniform lighting generated by array of light emitting diodes with large view angle". Optics express, 18(16): 17460-17476.

[23] Rakkolainen, I. K. and A. K. Lugmayr. 2007. "Immaterial display for interactive advertisements". Paper presented at Proceedings of the international conference on Advances in computer entertainment technology, at Salzburg, Austria.

[24] Sexton, I. and P. Surman. 1999. "Stereoscopic and autostereoscopic display systems". Signal Processing Magazine, IEEE, 16(3): 85-99.

[25] Shibata, T. 2002. "Head mounted display". Displays, 23(1–2): 57-64.

[26] Smith, W. J. 2000. Modern optical engineering: the design of optical systems. McGraw Hill. ISBN 9780071363600.

[27] Srivastava, A. K., J. L. de Bougrenet de la Tocnaye and L. Dupont. 2010. "Liquid Crystal Active Glasses for 3D Cinema". Journal of Display Technology, 6(10): 522-530.

[28] Szold, A. 2005. "Seeing is believing - Visualization systems in endoscopic surgery (video, HDTV, stereoscopy, and beyond)". Surgical Endoscopy and Other Interventional Techniques, 19(5): 730-733.

[29] Taffinder, N., S. G. T. Smith, J. Huber, R. C. G. Russell and A. Darzi. 1999. "The effect of a second-generation 3D endoscope on the laparoscopic precision of novices and experienced surgeons". Surgical Endoscopy-Ultrasound and Interventional Techniques, 13(11): 1087-1092.

[30] Toichi, M., T. Sugiura, T. Murai and A. Sengoku. 1997. "A new method of assessing cardiac autonomic function and its comparison with spectral analysis and coefficient of variation of R–R interval". Journal of the Autonomic Nervous System, 62(1–2): 79-84.

[31] van Bergen, P., W. Kunert and G. F. Buess. 1999. "Three-dimensional (3-D) video systems: Bi-channel or single-channel optics?". Endoscopy, 31(9): 732-737.

[32] Wade, N. and M. Swanston. 2013. Visual Perception: An Introduction, 3rd Edition. Taylor & Francis. ISBN 9781848720435.

[33] Wang, B., A. M. Goodpaster and M. A. Kennedy. 2013. "Coefficient of variation, signal-to-noise ratio, and effects of normalization in validation of biomarkers from NMR-based metabonomics studies". Chemometrics and Intelligent Laboratory Systems, 128(0): 9-16.

[34] Welling, W. 1978. Photography in America: The Formative Years, 1839-1900. University of New Mexico Press. ISBN 9780826309532.

[35] Wu, H.-H. 2007. "Rectification of stereoscopic video for planar catadioptric stereo systems". Circuits and Systems for Video Technology, IEEE Transactions on, 17(6): 686-698.

[36] Younwoo, B. 2011. Development and Applications of Optical Imaging Systems and Methodologies for Cross-Evaluation of Skin Lesions. Graduate School of Yonsei University, Biomedical Engineering.

8. Abstract (in Korean)

기존의 3 차원 영상 시스템의 (SIS) 경우 2 개의 다른 카메라를 사용하여 3 차원 영상을 획득하게 되어 있다. 하지만 2 개의 다른 카메라를 사용한 영상 시스템 (dual channel)의 경우 카메라 및 영상의 특성 차이에 의해서 구성된 3 차원 영상을 관찰하는 관찰자가 시각적 피로 (시각적 피로, 어지러움, 두통 등)를 느낄 수 있다. 특히 1) 카메라 영상 특성의 차이, 2) 카메라 시스템의 물리적 구성 차이로 인하여 시각적 피로가 발생한다. 또한 카메라 2 개를 사용하므로 1 개의 카메라를 사용했을 때 보다 부피가 상대적으로 클 것으로 예상 된다. 이를 해결하기 위해 카메라 1 개의 사용하여 물리적 부피를 줄이고 더불어 관찰자의 불편함을 제거 할 수 있는 단일 카메라 광학계를 구성하고 3 차원 영상을 획득 할 수 있는 시스템을 개발했다.

3 차원 영상의 기초가 되는 좌안, 우안 영상의 시차 만들기 위해 편향판을 (TRD) 사용하고 이를 사용한 영상 시스템의 가능성을 광학 시뮬레이션과 실험을 통하여 확인하였다. 편향판의 재질, 두께 및 회전 각도에 따른 분석을 시뮬레이션을 서로 다른 굴절률을 가지는 다이아몬드, acryl, BK7 를 10, 20, 30mm 의 두께로 가정하여 시뮬레이션을 진행함. 수동 회전을 하는 TRD 기반의 3 차원 영상 시스템 (TRD-SIS)를 설계하여 실험 결과를 비교함.

시뮬레이션 결과를 바탕으로 BK7 을 사용한 30mm 두께의 편향판을 사용하여 실시간 3 차원 영상 시스템을 개발 하였다. 카메라, 모터, active shutter glasses, 3 차원 display, AtMega128 (MCU)를 사용한 실시간 3 차원 영상

시스템을 (RT-TRD-SIS) 구성하였다. 특히 MCU 를 사용하여 중앙제어시스템을 구현하였고 프로그래밍을 통하여 제어를 하였다.

실시간 영상 획득을 하기 위해 편향판을 모터에 부착하고 24Hz (48 fps) 이상으로 회전시켜 시차를 연속적으로 관찰 가능하게 한다. 투명판 회전 후 시차를 발생 시킨 순간에 영상 획득을 해야 하기 때문에 카메라의 하드웨어 트리거 (trigger) 기능을 사용하여 필요한 시간 및 위치에서 영상을 획득하였다. 획득한 실시간 영상은 LabView 를 통하여 모니터에서 3 차원 영상을 디스플레이 (display) 하고 이를 관찰하기 위해 active shutter glasses 를 사용하여 영상 관찰을 가능하게 하였다.

구성한 시스템의 평가를 위해 두 가지 실험을 하였다: 작동 시간에 따른 온도 변화, 편향판 회전 각도에 따른 영상의 특성 분석. 장시간 모터의 동작 시 발생하는 열을 분석을 위해서 온도계와 열화상 카메라를 사용하여 추적하고 방열판과 팬을 사용하여 열을 제거하는 방법을 고안하였다. 또한 영상의 변동 계수 (coefficient of variation)를 통해 편향판의 회전에 따른 차이를 객관적으로 분석했다.

본 연구를 통하여 1 개의 카메라와 편향판을 사용하여 좌우 영상의 시차를 확인하고 이를 기반으로 실시간 3 차원 영상 시스템를 개발하였다. 또한 시스템 평가를 통해 시스템의 성능을 객관적으로 평가하였다.

Keywords: 3 차원 영상, 입체 영상, 편향판

APPENDIX A. COEFFICIENT OF VARIATION

```
% clear/close memory, figure, command in Matlab
clear all
close all
clc

% Load image file
a1=imread('00.jpg');

% calculate coefficient of variation (CV).
b2 = rgb2gray(a2);
c1=mean(b1);
d1=mean(c1);
e1=std2(b1);
cv1=(e1/d1)*100

% set plot setting
figure1 = figure;
axes1 = axes('Parent',figure1,'FontWeight','bold','FontSize',20);
xlim(axes1,[0 3456]);
box(axes1,'on');
hold(axes1,'all');

% plot calculated CV
set(plot(c1),'Color',[0 0 0],'DisplayName','00','LineWidth',1);
xlabel('Pixel Location','FontWeight','bold','FontSize',20);
ylabel('Intensity','FontWeight','bold','FontSize',20);
legend1 = legend(axes1,'show');
set(legend1,'Orientation','horizontal','Location','NorthOutside');
```